AN EVALUATION OF THE EFFECT OF INSTALLED CALORIMETERS ON THE IMPINGING HEAT FLUX DENSITY

Final Report

MS-1

to

National Aeronautics and Space Administration
George C. Marshall Space Flight Center
Huntsville, Alabama

Contract No. NAS8-5196

SOUTHERN RESEARCH INSTITUTE

2000 9th Avenue S. Birmingham 5, Alabama

AN EVALUATION OF THE EFFECT OF INSTALLED CALORIMETERS ON THE IMPINGING HEAT FLUX DENSITY

Final Report

to

National Aeronautics and Space Administration
George C. Marshall Space Flight Center
Huntsville, Alabama

Contract No. NAS8-5196

Southern Research Institute
Birmingham, Alabama
7351-1481-9-XL
July 13, 1965

TABLE OF CONTENTS

AN EVALUATION OF THE EFFECT OF INSTALLED CALORIMETERS ON THE IMPINGING HEAT FLUX DENSITY

INTRODUCTION

The initial concept of Task Order 9 was to investigate the effect of the size of calorimeters on the impinging heat flux densities at or near the exit of rocket engines. Preliminary calculations revealed that the size of the sensor might not be so important, but that the temperature of the sensor relative to its surroundings could have a large influence on the impinging heat flux density. Therefore, the purpose of this task order was to investigate analytically and experimentally the effects of both sensor temperature and size on the impinging heat flux density.

Specifically, the study was to determine both analytically and experimentally whether a calorimeter mounted in a plane wall having a higher surface temperature than the calorimeter will indicate an erroneous heat flux density as a result of the surface temperature difference, and to determine whether the size or location of the calorimeter has any influence on the error.

In order to predict the effect of surface temperature differences on the total heat flux density, it is necessary to consider the effect which this has on each of the various modes of heat transfer existing in the flight installation, and then relate the change, or error, in each, to the total heat flux density sensed by the calorimeter.

The effect of surface temperature discontinuities on the local convective heat transfer coefficient to a flat plate has been studied by several investigators.[1-6] The general conclusion has been that a surface temperature discontinuity results in a marked change in the convective heat transfer coefficient in the region of the discontinuity.

Rubesin[1] derived expressions for the heat transfer coefficient to a flat plate downstream of a surface temperature discontinuity for the case of a turbulent, incompressible boundary layer. He determined the constants in his equations from an experimental investigation by Scesa.[2] Other investigators[3-5] have since determined expressions similar to Rubesin's but having different exponential constants. Reynolds, Kays, and Kline[5] concluded from theoretical and experimental investigations that the Rubesin equation predicts heat flux densities which are too high, a conclusion which has since been substantiated by data reported by Eichorn, Eckert, and Anderson.[6]

From Rubesin's analysis and their own experimental investigation, the Advanced Technology Division (ATL) of American Standard concluded that large surface temperature discontinuities could cause the heat flux density indicated by a membrane calorimeter to differ by as much as 30 to 40% from the heat flux density to an isothermal surface.[7-9] The difference, they concluded, is due to a change in the heat transfer coefficient near the discontinuity. Their experimental investigation was performed using a C-1118 membrane calorimeter mounted in a copper plate to simulate the isothermal case, and in firebrick and ceramic-coated surfaces to simulate the nonisothermal case. Variable heating rates were provided by an oxy-acetylene torch directed parallel to the surface.

From similar tests on a nickel slug calorimeter, ATL concluded that their calibrations using both radiative and convective sources were similar until the heat flux density exceeded 15 $Btu/ft^2/sec$.

A preliminary analysis made here revealed that the major influence is not size of the sensor, but the temperature of the sensor relative to the surrounding material, so the subsequent analysis was directed toward the effect of surface temperature differences between the calorimeter and its surroundings on the impinging heat flux density. The analysis was based on turbulent, incompressible flow over a flat plate. It was concluded that solely because of the differences in the temperature of the sensor and its surroundings a colder calorimeter would be exposed to as much as 40% greater total heat flux density (radiation plus convection) for the case of any sensor at, say, 300°F with the surroundings at 1700°F to 3000°F. Also, slug and membrane calorimeters (of the same or different sizes) at greatly different surface temperatures of perhaps 1200°F would receive total heat flux densities different by as much as 30% when the convective fluid was at 4000°F. At flame temperatures of 6000°F, this difference would be of the order of 15% due to the increased influence of the radiative heat flux density, but the absolute error would remain approximately 40%. A further error results from the increase in the convective heat transfer coefficient in the vicinity of the discontinuity; however, it was suspected that this increase is far less than predicted theoretically by Rubesin[1] and discussed by ATL.[7-9]

The extent of the analytical studies made under this task order were limited due to commitments on other task orders. Hence, the analysis was not made in sufficient depth to predict the exact effect of a surface temperature discontinuity existing at a calorimeter imbedded in a surface which was at

a higher temperature. The analysis does point out, however, that differences in calorimeter temperatures can cause large differences in the heat flux densities regardless of the change in the heat transfer coefficients.

Experimental studies were performed on copper slug total calorimeters mounted side by side in an isothermal surface. The relative effects of calorimeter surface temperature and size on the impinging heat flux density were studied by designing the sensors to operate at different surface temperatures or by varying the size of the calorimeters.

THEORY

By independent analyses, several investigators[3-5] developed the following expression for the heat transfer coefficient downstream of a step temperature discontinuity

$$h = h_\infty \left[1 - \left(\frac{L}{X}\right)^{\frac{9}{10}} \right]^{-\frac{1}{9}} \qquad (1)$$

where h is the heat transfer coefficient downstream of the discontinuity, h_∞ is the heat transfer coefficient which would exist if the surface were isothermal and L and X are shown in the sketch below.

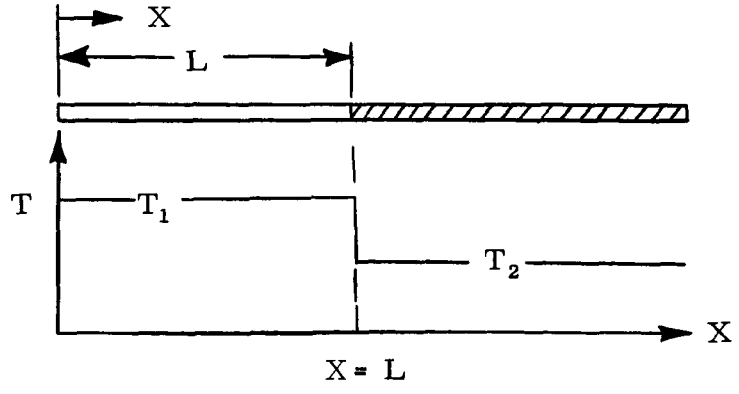

Equation (1) applies to turbulent incompressible flow over a flat plate with an unheated starting length ($T_1 = T_\infty$, where T_∞ is the free-stream temperature). Rubesin arrived at the same expression as equation (1) with the exception that the values of exponents were different:

$$h = h_\infty \left[1 - \left(\frac{L}{X}\right)^{\frac{39}{40}}\right]^{-\frac{7}{39}} \qquad (2)$$

Rubesin also extended his analysis to the case where the region of the plate preceeding the discontinuity was at a temperature other than the free-stream temperature ($T_1 \neq T_\infty$). The expression which he obtained was

$$h = h_\infty \left\{ \frac{T_1 - T_\infty}{T_2 - T_\infty} + \frac{T_2 - T_1}{T_2 - T_\infty} \left[1 - \left(\frac{L}{X}\right)^{\frac{39}{40}}\right]^{-\frac{7}{39}} \right\} \quad L < X \leq W \qquad (3)$$

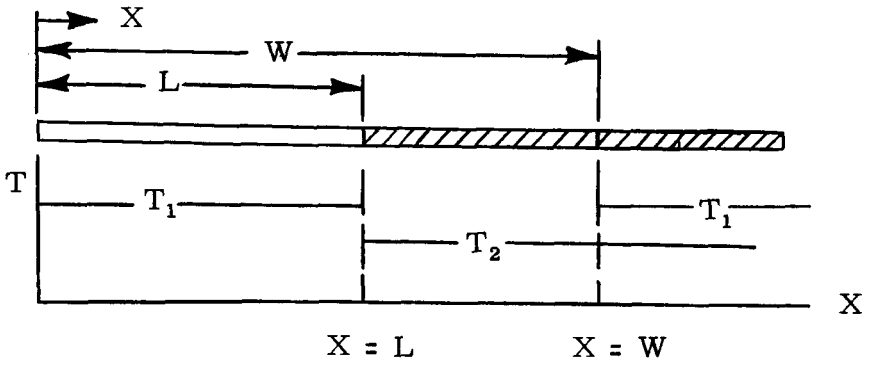

Further, Rubesin integrated and averaged equation (2) to yield the ratio of the average heat transfer coefficient over the region of the discontinuity (W-L) to the local heat transfer coefficient which would exist at the center of the region if the entire surface were at a uniform temperature T_1.

$$\frac{\bar{h}}{h_\infty} = F\left(\frac{L}{X}\right) + H\left(\frac{L}{X}\right) Z \qquad (4)$$

where $\bar{h}$ is the average heat transfer coefficient over the region $L < X \leq W$, h_∞ is the local isothermal heat transfer coefficient which would exist at $\frac{W+L}{2}$, L is the distance from the leading edge to the discontinuity, W is the distance from the leading edge to the rear of the region considered and Z is defined by

$$Z = \frac{T_2 - T_1}{T_2 - T_\infty} \qquad (5)$$

where T_2 is the temperature downstream of the discontinuity, T_1 is the upstream surface temperature and T_∞ is the free-stream temperature. The functions $F\left(\frac{L}{W}\right)$ and $H\left(\frac{L}{W}\right)$ in equation (4) are plotted on Figures 1 and 2, respectively.

It should be noted that W in equation (4) is actually a distance parameter which may be varied to change the dimensions of the region under consideration. The assumption is tacit in the equation that whatever values the surface temperature may have downstream of W will not effect the heat transfer coefficient upstream of W. The importance of the parameter W is that it is very useful in obtaining a theoretical expression for the average heat transfer coefficient over a small region. Rubesin stated that equation (4) could be applied to plug type heat meters installed in the surface of a flat plate. In the case of a plug type heat meter which was at a different temperature than the surface, L would be the distance from the leading edge to the front of the plug and W the distance from the leading edge to the rear.

The applicability of equation (4) to a small circular plug in a large plate is questionable in view of the fact that the analysis was made for a two dimensional boundary layer and does not include three dimensional effects which the discontinuities around the sides of the plug would introduce. Since this equation has not yet been satisfactorily correlated with experimental data for a circular plug type heat meter, the exact applicability of equation (4) to this situation is not known. However, experiments by ATL on circular transducers led them to conclude that Rubesin's analytical expression yielded values which approximated the experimental results.[7-9]

Values of the functions $F\left(\frac{L}{W}\right)$ and $H\left(\frac{L}{W}\right)$, as determined by Rubesin, indicate that this ratio will approach infinity as L/W approaches 1 (at the perimeter of a calorimeter). This seems somewhat contradictory to physical reality, and to some experimental data reported in reference 5. Undoubtedly, the so-called infinite transfer occurs over a finite distance and has but little effect on the average heat flux density into a sensor.

Since the heat flux density is given by the equation

$$\frac{q}{A} = k \left.\frac{\partial T}{\partial y}\right|_{y=o} \qquad (6)$$

where k is the thermal conductivity of the fluid in the boundary layer, and $\left.\frac{\partial T}{\partial y}\right|_{y=o}$ is the temperature gradient at the surface (at the calorimeter or the surroundings), Rubesin's equation predicts an infinite temperature gradient at the calorimeter surface near the discontinuity.

Reynolds, et al,[5] performed experimental measurements of velocity and temperature profiles in the boundary layer downstream of a step change in surface temperature. They found that near the discontinuity, the temperature profile departed from the predicted value; however, the heat transfer coefficients were increased on the order of 50% near the discontinuity, not infinitely as predicted. Thus, there is strong evidence to indicate that the theoretical equations break down near the discontinuity.

The following analysis shows that calorimeters at different temperatures may indicate considerably different heat flux densities. The purpose of the calculations is to indicate the magnitude of the error in the total heat flux density to calorimeters at surface temperatures different than the surroundings in which they are located. Note that the convective error in these readings would also be subject to an additional error in the heat flux density because of the increase in the heat transfer coefficient at the edges of the calorimeter due to the temperature discontinuity.

Consider the calorimeter to be a body embedded in a flat plate. The plate and calorimeter are assumed to be at constant, but different, surface temperatures. The calorimeter and surrounding plate are heated by a gas at temperature T_∞ flowing parallel to their surfaces with velocity u_∞. The velocity is assumed to be sufficiently high that a turbulent boundary layer exists next to the plate.

The net heat flux density to the calorimeter is given by the expression

$$\frac{q}{A} = e_s' \sigma (e_f T_\infty^4 - \alpha_f T_s^4) + h (T_\infty - T_s) \qquad (7)$$

where

$\frac{q}{A}$ = heat flux density, Btu/hr/ft^2

σ = Stefan-Boltzman constant = 0.173×10^{-8} Btu/hr/ft^2/°R^4

e_s' = effective emissivity of the surface $\frac{e_s + 1}{2}$

e_f = emissivity of flame

α_f = absorptivity of flame

T_∞ = gas temperature, °R

T_S = surface temperature, °R

h = convective heat transfer coefficient, Btu/hr/ft^2/°F

We shall now consider the net contribution of each of these terms for cases of a slug and a membrane calorimeter at surface temperatures of 1500°F and 300°F, and exposed to gas at 4000°F. The surrounding surface temperature is assumed to be 1700°F. Assume each calorimeter is 2 inches in diameter and that both are located 2 feet from the leading edge of the plate. These conditions correspond approximately to the test conditions reported by ATL.[7-9]

The radiant heat flux density will be calculated assuming an emittance and absorptivity of the flame equal to 0.2. For luminous flames, these values are conservative. The effective surface emittance e_s', based on an actual emittance of 0.9, is 0.95.

The radiant heat transfer to the slug calorimeter is then

$$q_r = e_s' \, e_f \, \frac{0.173}{3600} \left[\left(\frac{T_\infty}{100} \right)^4 - \left(\frac{T_S}{100} \right)^4 \right] \tag{8}$$

which gives a value of approximately 35 Btu/sec/ft^2 to the slug calorimeter and 36 Btu/sec/ft^2 to the colder membrane calorimeter, a difference of about 3 percent. As expected, for high flame temperatures, the lower surface temperature exerts little influence on the net radiant heat flux density.

To determine the heat flux density by convection, a convective heat transfer coefficient for the isothermal case will be determined. As an initial approximation, the effect of surface temperature discontinuities will be neglected.

Reynolds, Kays, and Kline[10] have shown that the local heat transfer coefficient for turbulent incompressible flow over an isothermal flat plate is given by the expression

$$Nu_x = 0.0296 \, Pr^{.6} \, Re_x^{.8} \left(\frac{T_S}{T_\infty} \right)^{-0.4} \tag{9}$$

where Nu_x is the local Nusselt number, Pr is the Prandtl number and Re_x is local Reynolds number.

The fluid properties are evaluated at the free stream static temperature. The ratio $(T_S/T_\infty)^{-0.4}$ in equation (9) is a correction for temperature dependent fluid properties. Equation (9) holds for Reynolds numbers from 10^5 to 3.5×10^6.

Although the fluid in this case is a mixture of the combustion products of oxygen and acetylene, in order to simplify the calculations, the properties of air will be used. Since the properties of air and most combustion gases are quite similar, this substitution will have little effect of the final results.

Recall that for flow over a flat plate, a boundary layer forms at the leading edge and increases in thickness with distance along the plate. The flow in the boundary layer is laminar for a critical distance X_c from the leading edge, beyond which it becomes turbulent.

The transition from laminar to turbulent flow usually occurs where the local Reynolds number is equal to 5×10^5. [11] For the purpose of this analysis, a value of 10^6 is assumed for Reynolds number.

The other properties of air at 4000°F are summarized below.

Pr = 0.8

k = 0.088 Btu/hr/ft²/°F

Substituting in equation (9) we get for the convective heat transfer coefficient

$$h = \frac{.0296\ (.088)\ (.8)^{.6}}{2}\ (10^6)^{.8}\ \left(\frac{1700}{4000}\right)^{-.4}$$

$$= 101 \text{ Btu/hr/ft}^2\text{/°F}$$

The heat flux densities to the two calorimeters (uncorrected for surface temperature discontinuities) is

$$\left(\frac{q}{A}\right)_{sc} = 101\ \frac{(4000 - 1500)}{3600} = 72 \text{ Btu/sec/ft}^2$$

to the warmer calorimeter, and

$$\left(\frac{q}{A}\right)_{mc} = 101 \frac{(4000-300)}{3600} = 104 \text{ Btu/sec/ft}^2$$

to the colder membrane calorimeter. The subscripts m and s refer to membrane and slug calorimeters, respectively; c denotes convection.

The results of these calculations are summarized in Table 1.

Thus, the total heat flux densities to the colder and warmer calorimeters are 140 and 107 Btu/ft^2/sec, respectively, a difference of approximately 30%. Note that this difference is due entirely to the difference in the surface temperatures of the two calorimeters. Also note from Table 1 that the true heat flux density to the surrounding surface at 1700°F is 100 Btu/sec/ft^2. The membrane and slug calorimeters thus indicate values which are 40% and 8% high, respectively.*

Returning to the basic heat flux density equation (7), consider the case of a typical flight installation, where the flame temperature T_∞ = 6000°F, and the surface temperatures are 300°F and 1500°F for the membrane and slug calorimeters, respectively. The surrounding surface temperature is assumed to be 3000°F.

The following fluid properties are assumed:

Pr = 1.0

k = 0.1 Btu/hr/ft^2/°F

$Re_x = 10^6$

A heat transfer coefficient of 123 Btu/hr/ft^2/°F was calculated and assumed as applicable to both the insulated surface and the calorimeter. The heat flux densities to the membrane and slug calorimeters were calculated to differ by 13%, which is considerably better agreement than for the prior case of lower flame temperatures. However, note that the heat flux densities to the calorimeters differ by 41.5% and 25.5% from the true heat flux density to the insulated surface. The effect of the calorimeter temperature on the impinging heat flux density is thus readily apparent even at the higher gas temperatures. The heat flux densities calculated from equation (7) are summarized in Table 2.

EXPERIMENTAL APPARATUS AND PROCEDURE

The experimental apparatus which was used in these studies is shown on Figure 3. This setup consisted of 1) a rectangular duct, 2) total and static pressure probes connected by a water manometer, 3) a gas temperature thermocouple, 4) two test transducers mounted side by side in the duct, and 5) recording devices to measure the voltage output of the transducers. An oxy-acetylene torch was used to provide a high temperature gas stream.

A rectangular duct was used in order to provide turbulent flow. It was found that the oxy-acetylene torch did not provide a sufficiently high velocity to yield turbulent flow over a flat plate for the length of duct space available. The duct dimensions were 3 inches by $\frac{1}{2}$ inch giving a hydraulic diameter of 0.856 inches. The ducts were constructed of firebrick coated with zirconium oxide cement (Zircona Y-82 Cement) with the exception of ducts 5 and 6. Duct 5 was constructed from zirconia plates and duct 6 was made of uncoated firebrick.

The total and static pressure probes were made of graphite and were used to measure the gas velocity. The probes were connected through a manometer so that the differential pressure could be read directly in inches of water. This reading was converted into flow velocity by using the definition of velocity head for incompressible flow.

$$V = \frac{gH\gamma}{12} \tag{10}$$

where g is the gravitational constant, H is the differential pressure in inches of water, γ is the ratio of the specific weight of water to the specific weight of the gas at the flow conditions and V is the velocity in ft/sec. The assumption of incompressible flow was valid at the low Mach numbers encountered.

The flow velocity was found to remain very constant during the run, thus the water manometer was acceptable as a measuring device. Furthermore, it was found that the gas velocities were fairly repeatable from run to run; therefore, gas velocities were measured only for the first two test ducts. For all following runs the velocity was assumed to be approximately that measured in the first runs. This procedure did not lead to any additional error since the only purpose of the velocity measurement was to confirm that turbulent flow existed in the duct.

The gas temperature was measured with an iridium/iridium-60 rhodium thermocouple. This couple was mounted through the isothermal wall and bent at a 90° angle such that it centered in the duct and was nearly isothermal for a short length to reduce conduction losses.

The isothermal (duct) surface temperature was measured with a chromel-alumel thermocouple mounted approximately $\frac{1}{64}$ inch below the duct surface. This couple was inserted through the firebrick, bent at an angle of 90°, and cemented in place during the buildup of the duct. The length of wire parallel to the duct surface of about $\frac{3}{4}$ inch long was placed in the leads to reduct conduction losses from the bead. In the last two ducts platinum/platinum-10 rhodium thermocouples were used to measure the surface temperature. These thermocouples were placed in a very small groove running across the duct with the bead located in the center and the leads extending to either side of the duct. This installation was found to work equally well if not better than the previous installation.

The slug calorimeters used are shown in Figure 4. As shown these slugs were made of copper and grooved to increase the effective emittance of the surface. Chromel-alumel thermocouples spot-welded to the back of these transducers provided the emf-time measurements used in the heat flux density calculations.

In order to measure surface temperature effects, two slug calorimeters of $\frac{1}{2}$ inch diameter were used; one being $\frac{1}{8}$ inch thick and the other $\frac{3}{8}$ inch thick. The thicker calorimeter had the lower temperature rise with time, therefore, providing the lower surface temperature. A theoretical analysis of the $\frac{3}{8}$ inch thick calorimeters was made to evaluate the temperature lag existing between the front and back face during transient heat flow. An analysis for an infinite slab insulated on the back face and with a constant heat flux density over the front face revealed that the temperature difference would be about 8°F; however, the temperature lag remains approximately constant with time, therefore, yielding the correct temperature-time slope for heat flux density calculations. The only error introduced is in the value of the specific heat used in the calculations, and this amounts to an error of only 0.3%.

For studying the effects of calorimeter diameters, calorimeters of $\frac{1}{2}$ inch and 1 inch diameters and $\frac{1}{4}$ inch and 1 inch diameters were used. These calorimeters were all $\frac{1}{8}$ inch thick so that under identical heat flux conditions they would exhibit the same temperature-time behavior.

Before making a run, the duct was constructed by coating firebrick with zirconium-oxide cement (Zircoa Y-82). During the buildup, the pressure probes and gas and surface temperature thermocouples were cemented in place. The duct was radiused on the front end as shown in Figure 3 to guide the flow from the oxy-acetylene flame. The tangent point of the radius and the straight run of the duct was taken as the leading edge for all measures of the location of the calorimeters.

The calorimeters were all weighed and measured before attaching the thermocouples. After these measurements, the thermocouples were attached and calibrated for temperature versus emf output against a standard thermocouple. The calibrations were performed with the calorimeters attached to the galvanometer circuit of the oscillograph, which would be used during the test, and with the correct length of lead wire. This calibration then accounted for errors inherent in the thermocouple junctions as well as errors arising from current requirements of the oscillograph. After the calibration was complete, the calorimeters were installed in the duct and insulated on the sides and bottom with Fiberfrax with the exception of duct 6 for which thermatomic carbon insulation was used.

The test assembly was then positioned in front of the oxy-acetylene torch and all recording equipment connected. The outputs from the calorimeters and the surface temperature thermocouple were recorded on a Midwestern Instruments oscillograph, Model No. 621-5. The gas temperature was recorded on a Moseley X-Y recorder. The measurements taken were (1) the gas temperature, (2) the velocity head of the gas, (3) the emf versus time outputs of the two calorimeters and (4) the emf versus time output of the surface temperature thermocouple.

The heat flux density data were reduced from the temperature-time data of the calorimeters by using the following standard equation.

$$\frac{q}{A} = \frac{W}{A} C_p \frac{\Delta T}{\Delta \theta} \qquad (11)$$

where $\frac{q}{A}$ is the heat flux density in Btu/sec/ft^2, $\frac{W}{A}$ is the weight to cross-sectional area ratio of the calorimeter in lb/ft^2, C_p is the specific heat of copper in Btu/lb/°F and $\Delta T/\Delta \theta$ is the slope of the temperature-time curve at a given time in °F/sec. The values used for the specific heat of copper were taken from WADC TR-58-476 and are shown on Figure 5.

Since the objective was to study the effects of thermal disturbances on the convective heat flux, the radiation heat flux density had to be separated from the total heat flux density measured by the test calorimeters. To determine the radiation heat flux density, a radiation calorimeter was used. The calorimeter (Chrysler Corporation Model N-118-6460 Serial No. 162) utilized a copper slug calorimeter mounted in a stainless steel housing. The calorimeter was separated from the flowing gas by a quartz window and a helium purge was directed across the outer surface of the window. The radiation calorimeter was calibrated against our "standard" copper slug calorimeter for three different purge flow rates, and the measured heat flux was found not to depend on the flow at the small flow rates used. The calorimeter was then installed in the duct, and the heat flux density was measured at the approximate location at which the total heat flux sensors were installed. From the radiation measurements, a curve of heat flux density versus the surface temperature of the duct was obtained. The data obtained indicated that the radiation from the CO_2, CO and H_2O gases in the oxy-acetylene flame was 6.5 Btu/sec/ft^2 and was approximately constant for duct surface temperatures from 0 to 550°F. Above 550°F, the gas radiation was augmented by radiation from the upper duct surface which increased in a power curve with temperature. The radiant heat flux density as a function of duct surface temperature and a given gas temperature is shown on Figure 6. These experimental data were used to obtain a convective heat flux density by subtracting the radiant portion which impinged on the calorimeter at a given duct surface temperature from the total measured heat flux density indicated by the slug calorimeters.

DATA AND RESULTS

Data were obtained on six different ducts which represented six different experimental setups. A total of 19 runs were made of which 10 were considered valid. Table 3 gives all of the pertinent information on the runs with regard to calorimeter size, location in the duct and the number of runs made with each experimental setup. Typical temperature-time data for an experimental run are shown in Figure 7. All of the data obtained were not reduced and presented since obvious errors were apparent in some of the readings due to various causes such as calorimeter insulation, loss of a calorimeter or thermocouple indication, etc.

The data are presented in Tables 4 through 7. The measured heat flux densities were calculated by applying equation (11) to the calorimeter data. The radiant heat flux densities were then subtracted from the

measured heat flux densities to yield the desired convective data. The value of the radiant heat flux density was obtained from Figure 6 which gives the radiant heat flux density to a calorimeter as a function of the wall temperature. The convective heat transfer coefficient was calculated from the equation

$$h = \frac{q_c}{T_\infty - T_c} \tag{12}$$

where

h = heat transfer coefficient, Btu/sec/ft^2/°F

q_c = convective heat flux density, Btu/sec/ft^2

T_∞ = gas temperature, °F

T_c = calorimeter surface temperature, °F

The theoretical ratio of the average heat transfer coefficient, $\bar{h}$, to the coefficient which would exist for an isothermal surface, h_∞, was calculated from Rubesin's equation (4). These ratios were determined for both calorimeters. The ratio of the average heat transfer coefficients for the two calorimeters was obtained by dividing the two ratios $\bar{h}/h_\infty$. All three ratios are presented in Tables 4 through 7.

The purpose of the runs made in ducts 2 and 3 was to ascertain the effect of a surface temperature discontinuity on the convective heat flux densities measured by calorimeters at different temperature. The two calorimeters used in these runs were $\frac{1}{8}$ inch and $\frac{3}{8}$ inch thick, respectively. These runs were made in a firebrick duct which was coated with zirconium oxide cement. Both calorimeters were made the same diameter in order to isolate the temperature effects from effects of calorimeter size or location.

Typical time-temperature plots for these runs are shown in Figure 7. The convective heat flux densities measured by the two calorimeters are shown in Figures 8, 9, 10, and 11. Also shown on the upper portion of the figures is the difference in the surface and calorimeter temperature for each of the calorimeters. Note that the higher temperature difference represents the colder calorimeter since the surface temperature was the same relative to each calorimeter.

Composite plots of the measured heat flux densities for the runs in ducts 2 and 3 are shown in Figures 12 and 13, respectively. For all of these runs the calorimeter with the lower temperature indicated a higher convective heat flux density. Note that the difference in the convective heat flux densities between the two calorimeters was considerably greater in duct 3 than in duct 2. The reason for this is not known but probably relates to the physical aspects of the system.

Shown on Figures 14 and 15 are the ratios of the heat transfer coefficients of the lower to the higher temperature calorimeter for ducts 2 and 3 respectively. Also shown on these figures is the theoretical ratio as predicted by Rubesin. Note from Tables 4 and 5 that Rubesin's analysis predicted a very small change in the average heat transfer coefficient over that which would exist if the surface were isothermal, hence the predicted ratio was also small. This was due mostly to the fact that the surface temperature did not reach sufficiently high temperatures to cause a large predicted change.

The ratios shown in Figure 14 for duct 2 were scattered about the values predicted by Rubesin; however, this was rather inconclusive since very little change was predicted. The ratios on Figure 15, however, were considerably higher than those predicted by Rubesin. Theoretically one would expect that the ratio of the heat transfer coefficients would increase as the temperature discontinuity increased. This behavior was exhibited slightly for the runs in duct 2 and a very definite trend in that direction was noted up to 8 seconds for run 1 in duct 3. However, run 2 in duct 3 exhibited exactly the opposite behavior, decreasing with an increasing discontinuity.

On Figures 16 and 17 the measured average heat transfer coefficients are compared with the theoretical isothermal heat transfer coefficients and the nonisothermal heat transfer coefficients as predicted by Rubesin for ducts 2 and 3 respectively. Shown on these figures are the measured average heat transfer coefficients, the theoretical local heat transfer coefficient which would exist at the center of the calorimeters if the surface were isothermal at the surface temperature, as predicted by the analysis of Reynolds, et al,[10] equation (9), and the theoretical average heat transfer coefficients as predicted by Rubesin, equation (4), based on the above mentioned isothermal local heat transfer coefficient, h_∞. Note that the agreement between the measured and the theoretical values was poor. In fact, generally, the curve of the measured average heat transfer coefficients exhibited an entirely different character from the curves of the theoretical values.

Shown on Figure 18 are the measured convective heat flux densities to calorimeters of different diameters. One calorimeter was $\frac{1}{2}$" diameter and the other was 1" diameter. They were made to have the same $\frac{W}{A}$ ratios so that under identical heat fluxes they would maintain identical temperatures thus allowing the size effect ($\frac{L}{W}$ ratio) to be studied. These runs were made in a duct of firebrick coated with zirconium oxide cement.

Note from Figure 18 that there was very little difference in the convective heat flux densities measured by the two calorimeters. The heat flux densities could be considered identical within the data scatter.

Shown on Figure 19 are the ratios of the average heat transfer coefficients of the 1" diameter to the $\frac{1}{2}$" diameter calorimeters. Also shown on this figure is the theoretical ratio as predicted by Rubesin. Note from Table 6 that Rubesin predicted very little difference (less than 10 percent) between the average heat transfer coefficients to the two calorimeters, hence the predicted ratio was very nearly 1. The small predicted theoretical differences in the average heat transfer coefficients to the two calorimeters was a result of small temperature discontinuities. Also the $(\frac{L}{W})$ ratios were not large enough to cause the function $H(\frac{L}{W})$ in equation (4) to override the function Z which stayed small due to the lower than desired surface temperatures. Since Rubesin predicted small differences and small differences were measured, these runs were not a good check of the theory.

In order to obtain large differences in the $(\frac{L}{W})$ ratios along with higher surface temperatures, $\frac{1}{4}$" and 1" diameter calorimeters were mounted in an uncoated firebrick duct. The convective heat flux densities measured in duct 6 for the $\frac{1}{4}$" and 1" diameter calorimeters are presented on Figure 20. The surface temperature discontinuities at each calorimeter are presented on the upper portion of this figure. Note that the surface temperature discontinuities obtained with this duct were much higher than those obtained on previous runs. Note also that the $\frac{1}{4}$" diameter calorimeter which had the larger $(\frac{L}{W})$ ratio indicated a considerably higher flux density. This was to be expected from the theory; however, the difference was much larger than predicted.

Shown on Figure 21 are the ratios of the average heat transfer coefficients of the larger $(\frac{L}{W})$ ratio calorimeter to the smaller $(\frac{L}{W})$ ratio calorimeter. Also shown on this figure is the theoretical ratio as calculated from Rubesin's theory. The measured ratio was much higher than that predicted by the theory. However, it is believed that a large portion of this difference resulted from experimental uncertainties due to the difficulties in locating a very small calorimeter parallel to the flow direction and in properly defining the insulation thickness.

A comparison of the measured average heat transfer coefficients with the theoretically predicted values for duct 6 is given on Figure 22. The local isothermal heat transfer coefficient used as an h_∞ base for the values predicted by Rubesin were calculated from equation (9) as before. The values measured with the larger $(\frac{L}{W})$ ratio calorimeter ($\frac{1}{4}$" dia. No. 7)

were considerably higher than the theoretically predicted values. The measured average heat transfer coefficient for the calorimeter with the smaller $(\frac{L}{W})$ ratio (1" dia - No. 9) were near the predicted values.

Because of the higher calorimeter temperatures attained in this last run, the effect of reradiation from the calorimeter surface was investigated. From calculations, the maximum reradiated energy was less than 4 percent of the incident radiant energy, so no correction was applied to the data.

CONCLUSIONS

Qualitatively, the data bear out the original conclusion that a lower surface temperature for a slug calorimeter results in a higher input convective heat flux density. The difference is greater than one would expect solely due to the temperature difference $(T_\infty - T_2)$ across the boundary layer. Thus, it can be concluded that the heat transfer coefficients to two calorimeters at different surface temperatures are not identical. There is some difference in the heat transfer coefficients probably resulting from edge discontinuities. A major portion of the differences in the measured convective heat flux densities, especially for duct 3, was attributed to experimental inaccuracies. These inaccuracies were a result of differences in insulation thickness, the effects of the grooved calorimeter surfaces, and the difficulty of correctly placing the calorimeters flush with the surface. Exactly what inaccuracy each of the above uncertainties contributed to the total error was not determined; however, no other explanation exists for the large differences in the measured convective heat flux density between calorimeters for one duct and the smaller differences for the other. Note that these same physical difficulties would be present when installing a total calorimeter in a flight vehicle.

For the runs in duct 4 concerning the effects of the $(\frac{L}{W})$ ratio, both the $\frac{1}{2}$" and the 1" calorimeters (same thickness) measured approximately the same convective heat flux density within the data scatter. Equation (4) predicted very little difference in the convective heat flux densities to the two calorimeters. One can only conclude that the $(\frac{L}{W})$ ratios used would not cause significant differences in the input heat flux density at the relatively low temperature (1000°F) of the surrounding material as used for this duct.

Higher duct temperatures and larger differences in the $(\frac{L}{W})$ ratios were obtained in duct 6 when using $\frac{1}{4}$" and 1" diameter calorimeters. However, the data obtained from the $\frac{1}{4}$" diameter calorimeters rendered the results of the

runs in these ducts questionable. The small calorimeter measured convective heat flux densities which were extremely high, much higher (perhaps 100 percent) than theoretically expected or observed in runs in other ducts. This leads one to the conclusion that the small size of the calorimeter compounded the installation errors. Any flow interference caused by the $\frac{1}{4}$" diameter calorimeters would have a much more pronounced effect on their readings than the same interference caused by the larger calorimeter on its readings. The run was not checked because the duct was destroyed.

RECOMMENDATIONS FOR FURTHER STUDY

The various causes of discrepancies in measured heat flux densities discussed in this report have included some which could be verified and some which were only conjectured. Whether all these factors, or only a few, are present in a given installation, it is quite difficult to separate and define them quantitatively so that they can be compensated for by suitable calibration procedures. Since most of these sources or error are directly related to temperature differences between the calorimeter and the surrounding surface, the more practical approach is to design the calorimeter so that its temperature rise matches that of the surroundings. This approach would have the additional advantage of reducing heat exchange with the surroundings, thus simplifying the problems of installation.

The surfaces in which the calorimeter are embedded experience a rapid temperature rise. Thus, the calorimeter, if it is to exhibit the same rise, must be capable of withstanding higher temperatures than the commonly used slug or membrane calorimeters, in order to permit monitoring through the entire flight.

One approach to this problem might be to use the base plate material itself as a heat flux density transducer. Such a calorimeter would not be subject to errors resulting from large temperature discontinuities at the boundary, but other problems would undoubtedly be incurred.

A second solution might be found through the use of a refractory material for the calorimeter, designed so that its temperature rise would match that of the surrounding insulation. The graphite thermocouple developed under Task Order 6 seems promising for this application. The calorimeter would have to be carefully designed to match the anticipated thermal conditions and mounting location; however, this approach appears to present fewer problems than the alternate one of attempting first to determine, and then to eliminate the several sources of error shown to accompany the use of low temperature transducers.

Another approach to the problem would be to mount the calorimeter in a disc of material that represented an infinite thermal boundary when mounted in the flight vehicle. This approach would permit precision mounting followed by careful calibration that would not be influenced by the surrounding thermal conditions in flight. Indeed, the output of the calorimeter could be calibrated for the "cold wall" heat flux density.

Submitted by:

E. D. Smyly

E. D. Smyly
Assistant Engineer
Thermodynamics Section

Approved by:

C. D. Pears

C. D. Pears, Head
Mechanical Engineering Division

7351-1481-9-XL
(10:12) lw

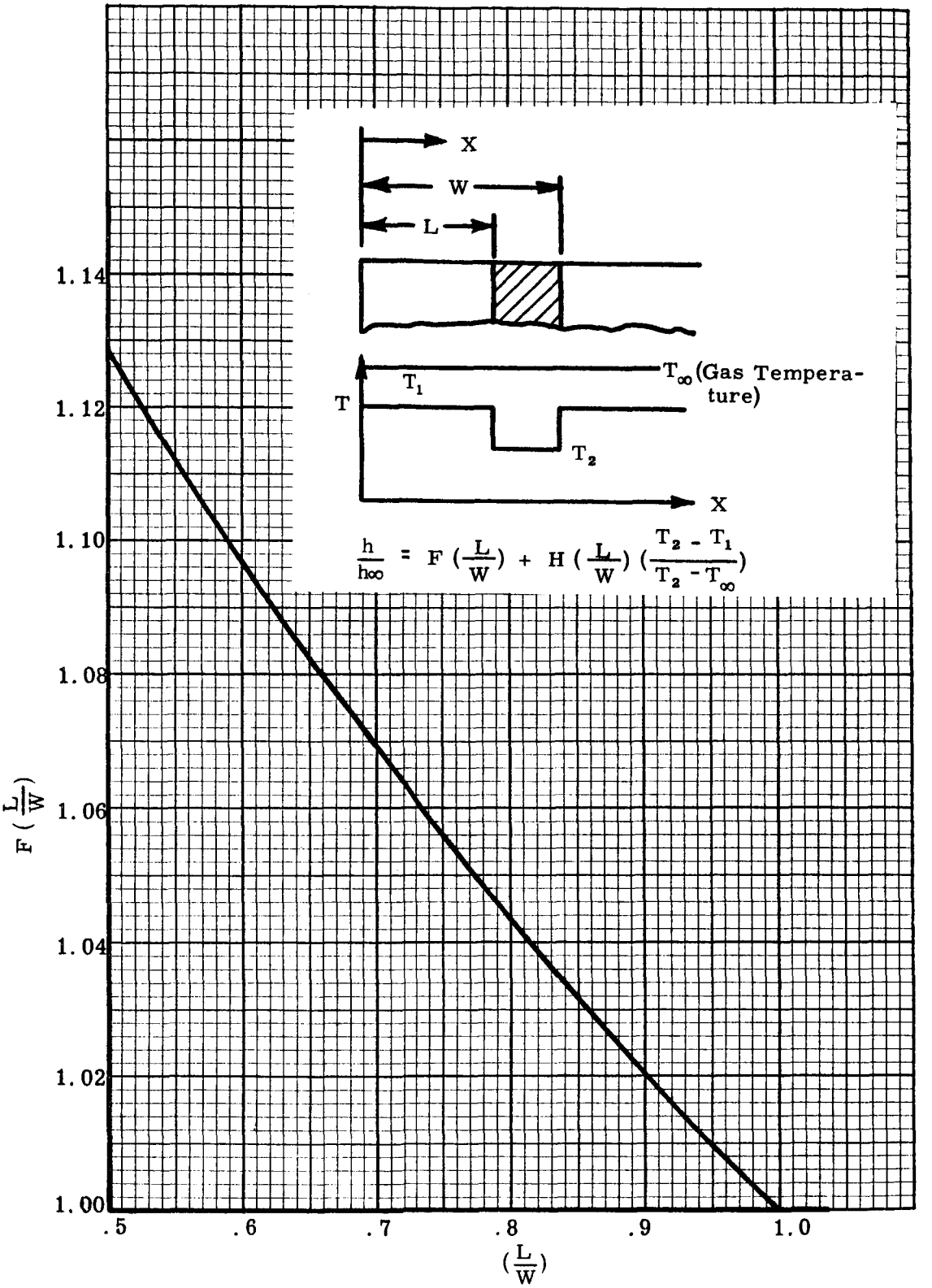

Figure 1. The Function F $(\frac{L}{W})$ Appearing in Rubesin's Equation

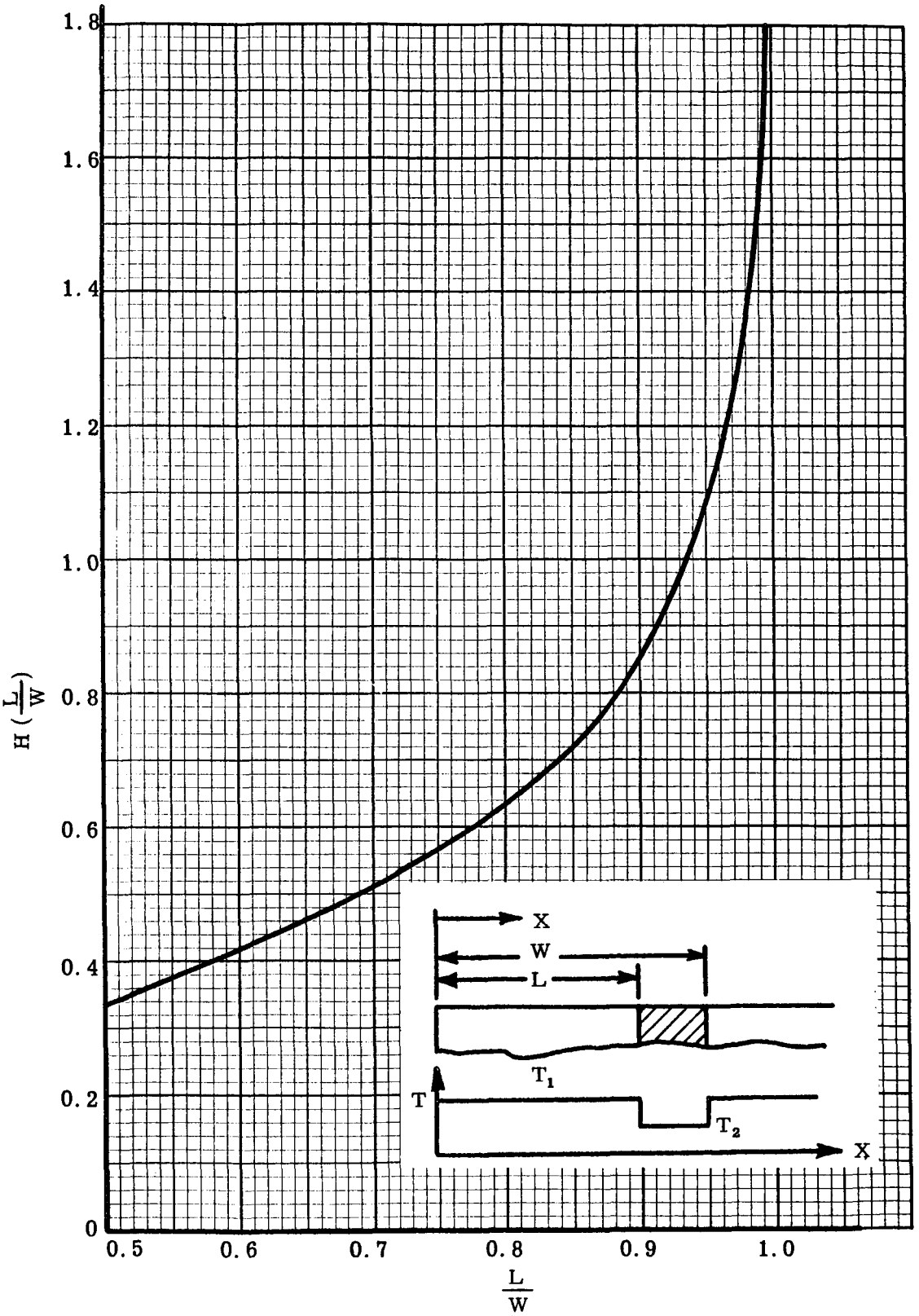

Figure 2. The Fuction H($\frac{L}{W}$) Appearing in Rubesin's Equation

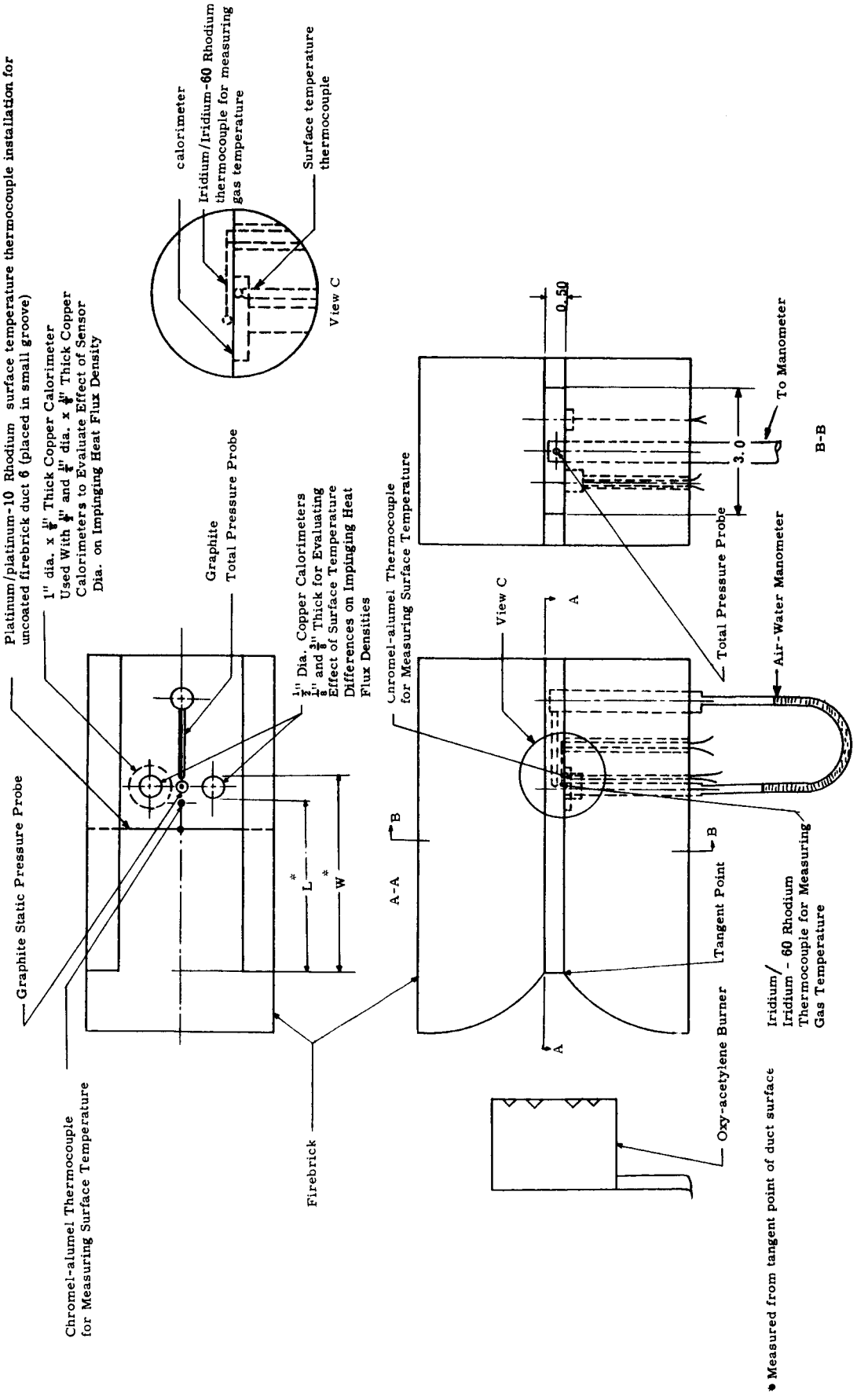

Figure 3. Experimental Apparatus Used in Evaluating Effect of Calorimeter Size and Surface Temperatures on Impinging Heat Flux Densities

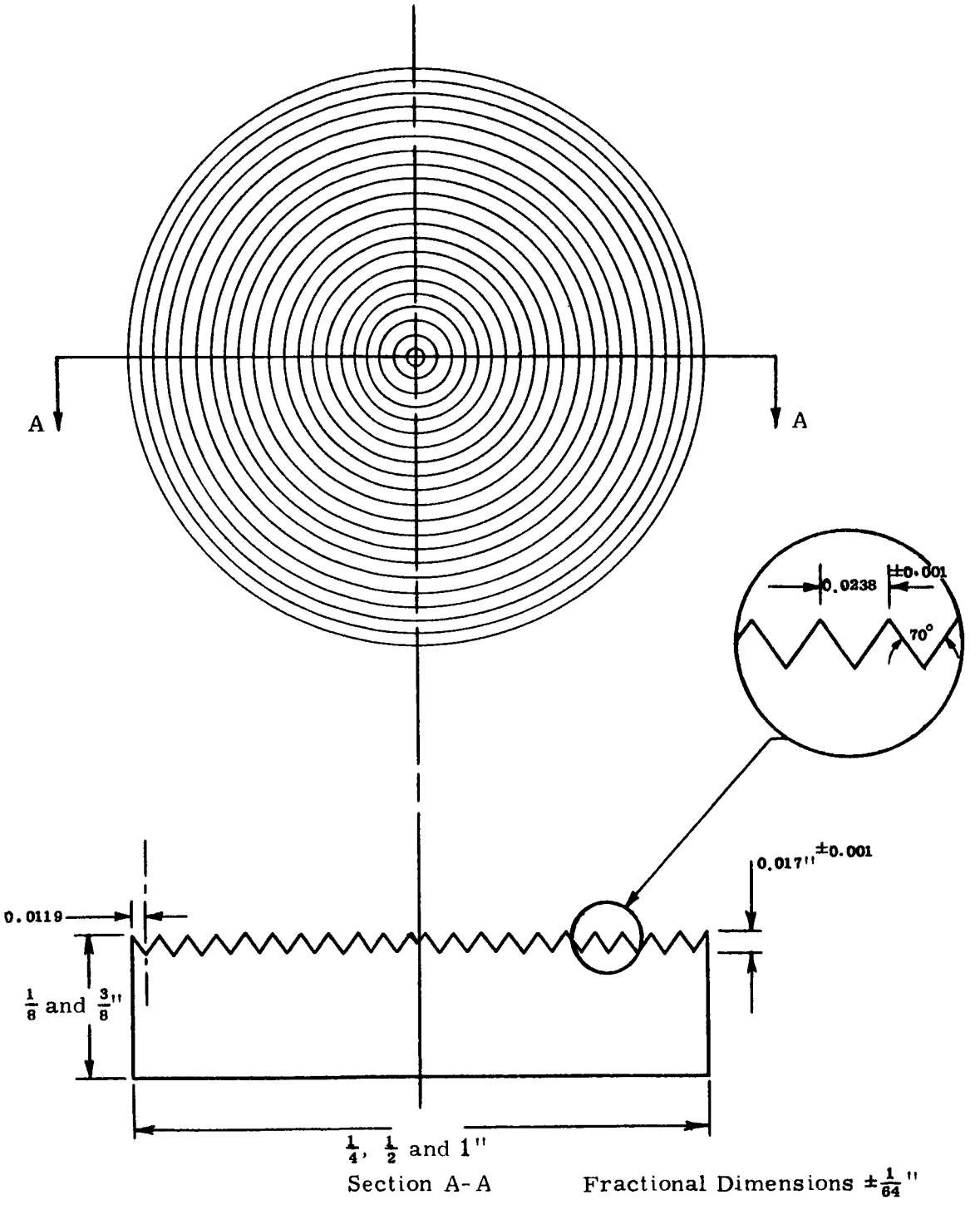

Figure 4. Copper Slug Calorimeters Used in Various Tests

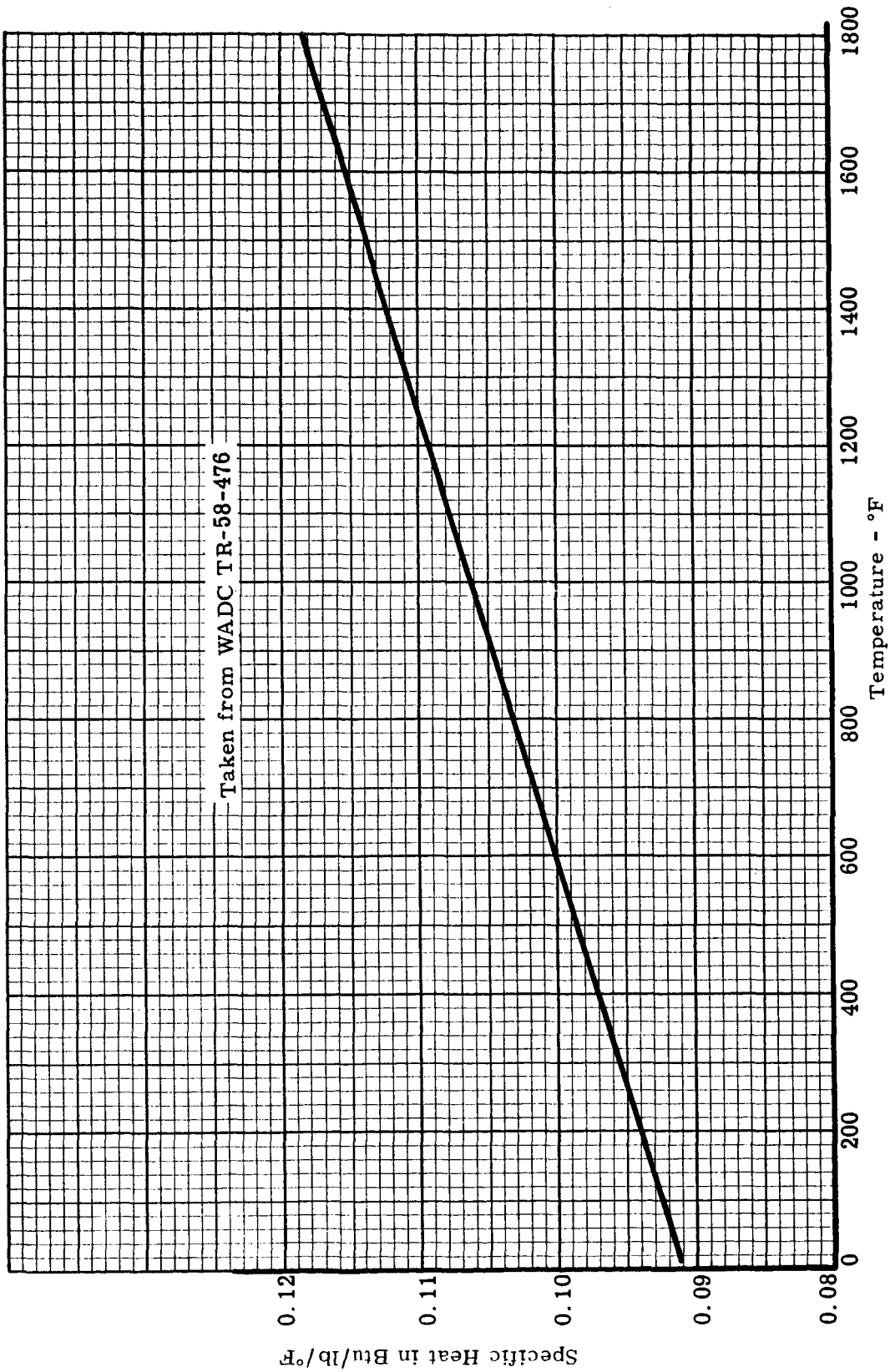

Figure 5. Specific Heat of Copper

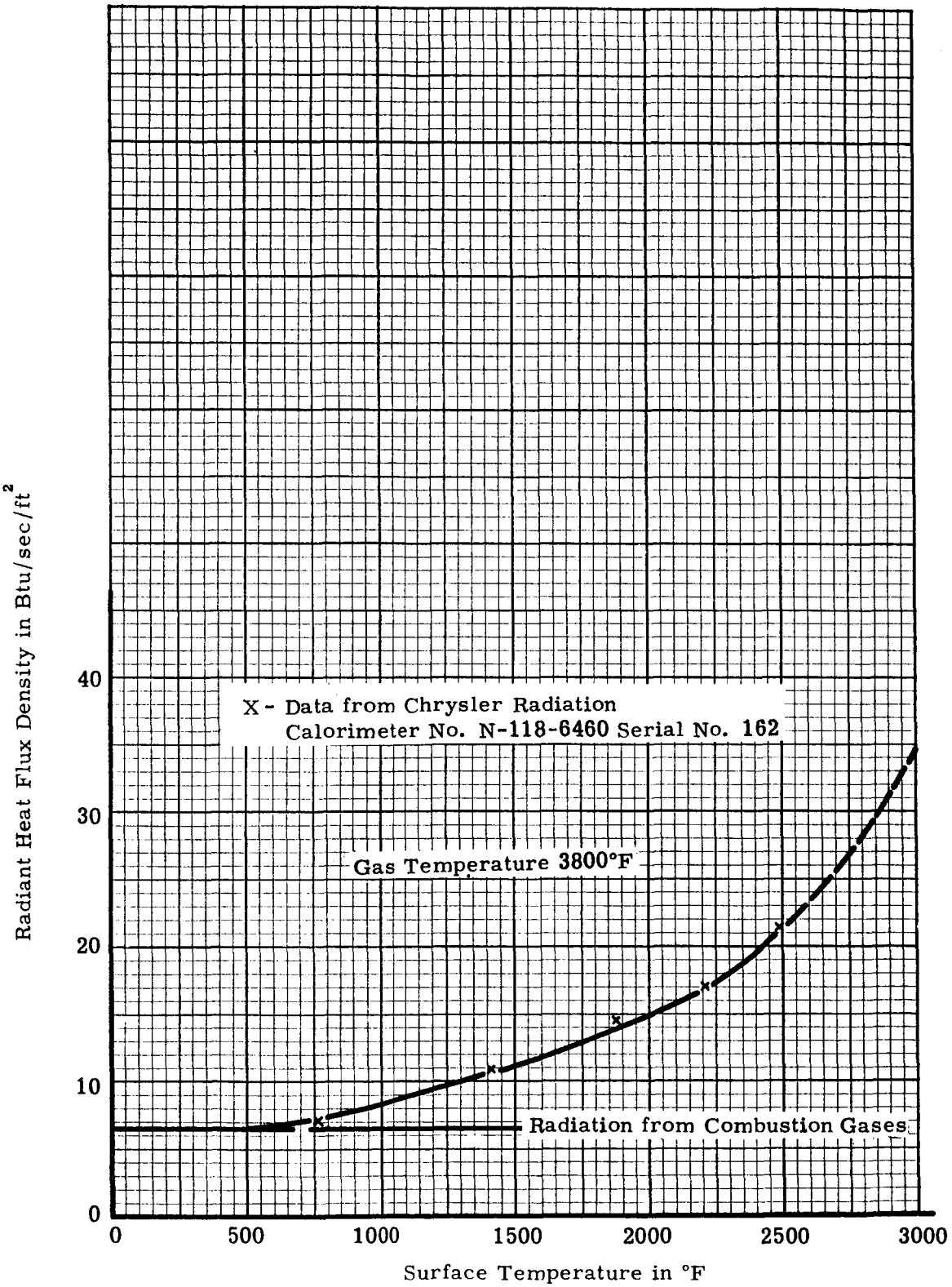

Figure 6. Radiant Heat Flux Density Received by Calorimeter (with window)

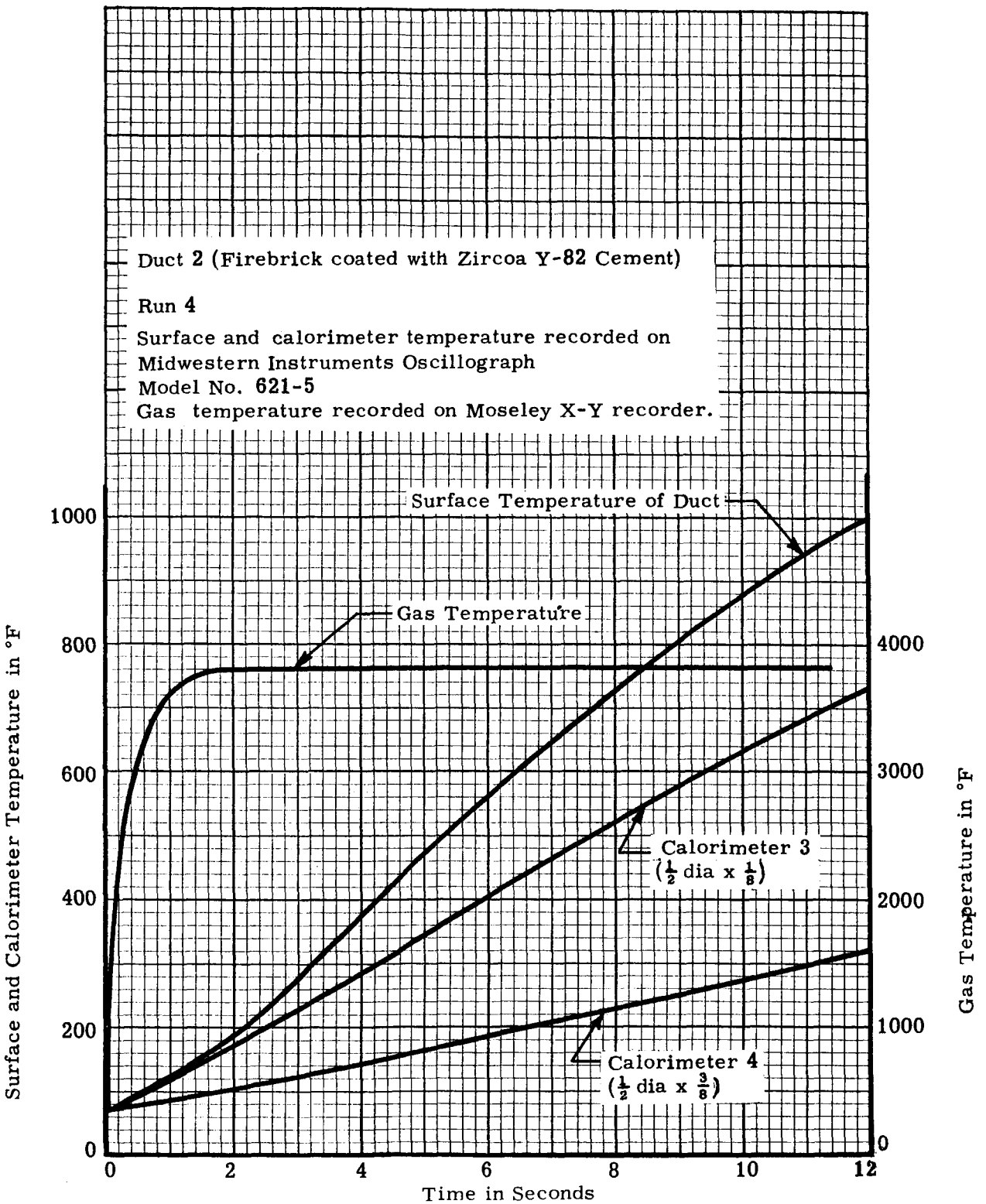

Figure 7. Typical Temperature-Time Data for Total Heat Flux Density Measurements

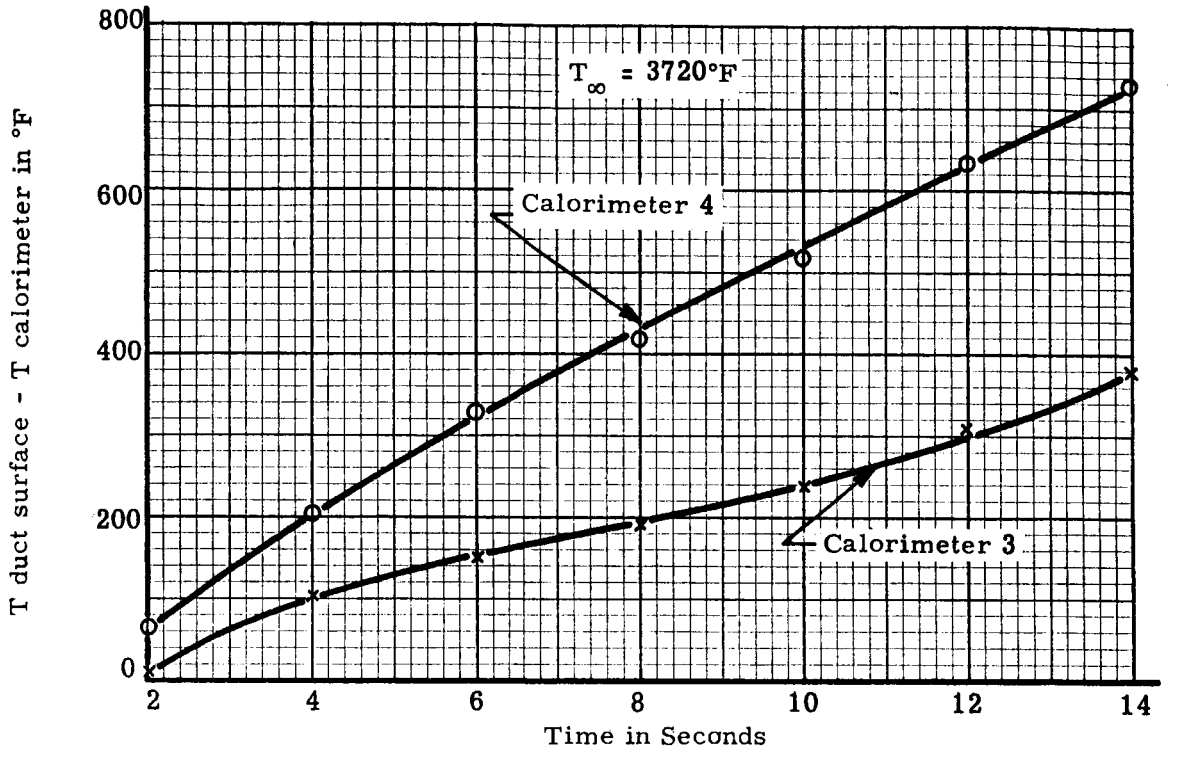

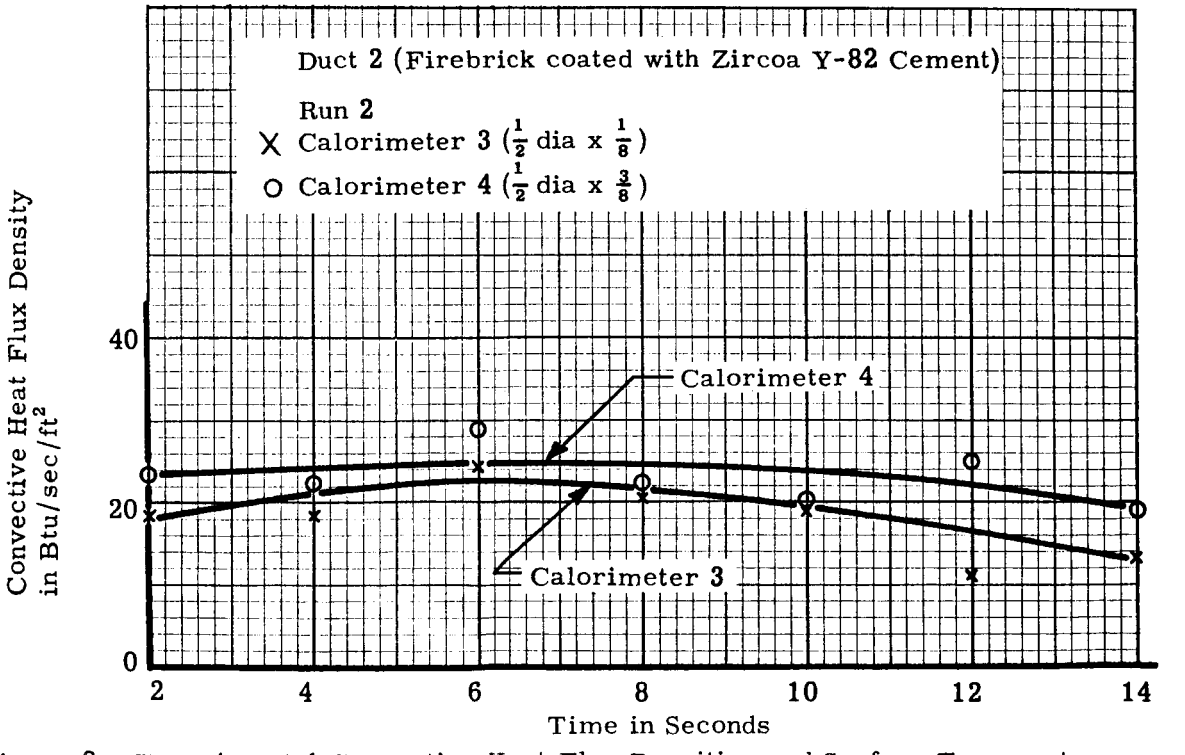

Figure 8. Experimental Convective Heat Flux Densities and Surface Temperature Discontinuities Measured by Slug Calorimeters with Different $(\frac{W}{A})$ Ratios–Duct 2

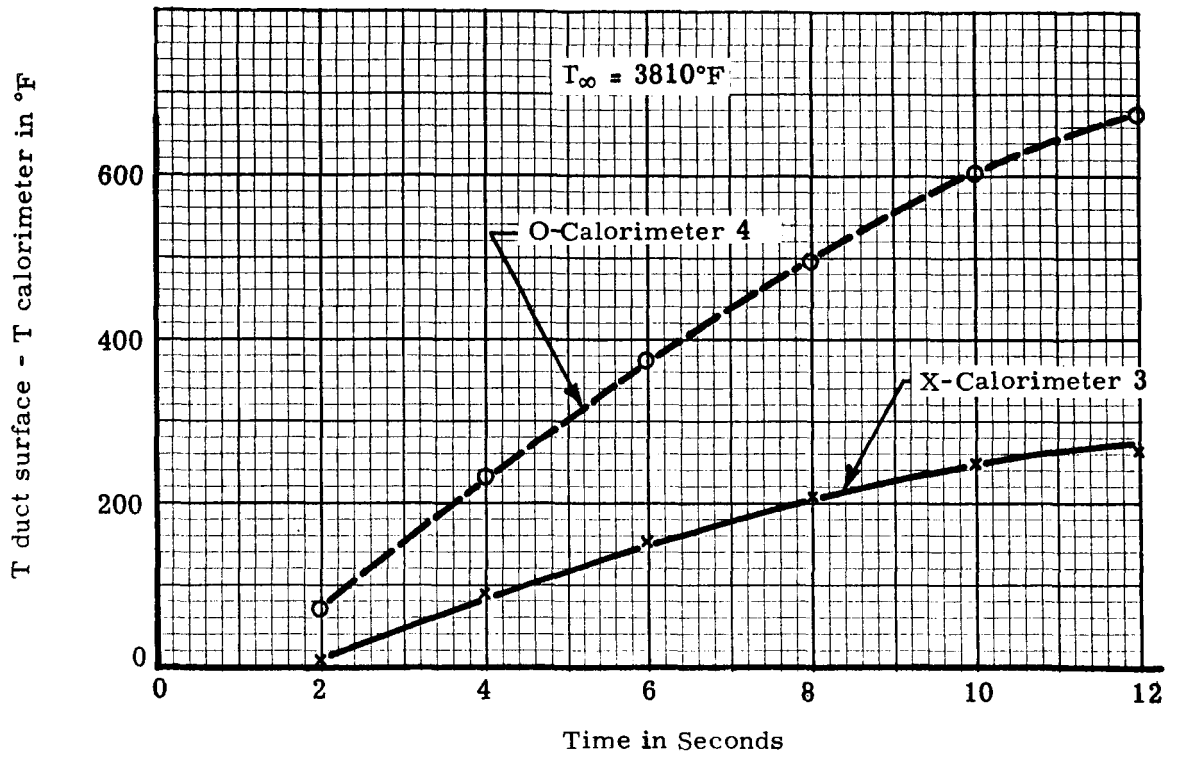

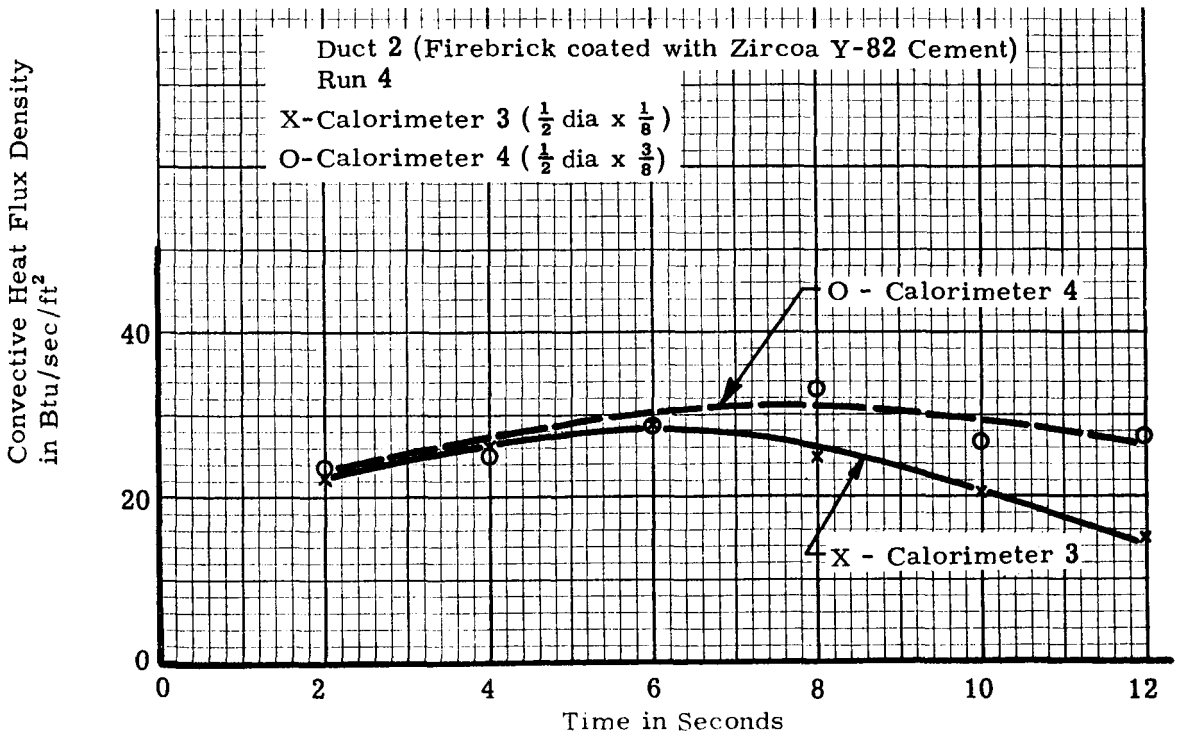

Figure 9. Experimental Convective Heat Flux Densities and Surface Temperature Discontinuities Measured by Slug Calorimenters with Different $\left(\frac{W}{A}\right)$ Ratios —Duct 2

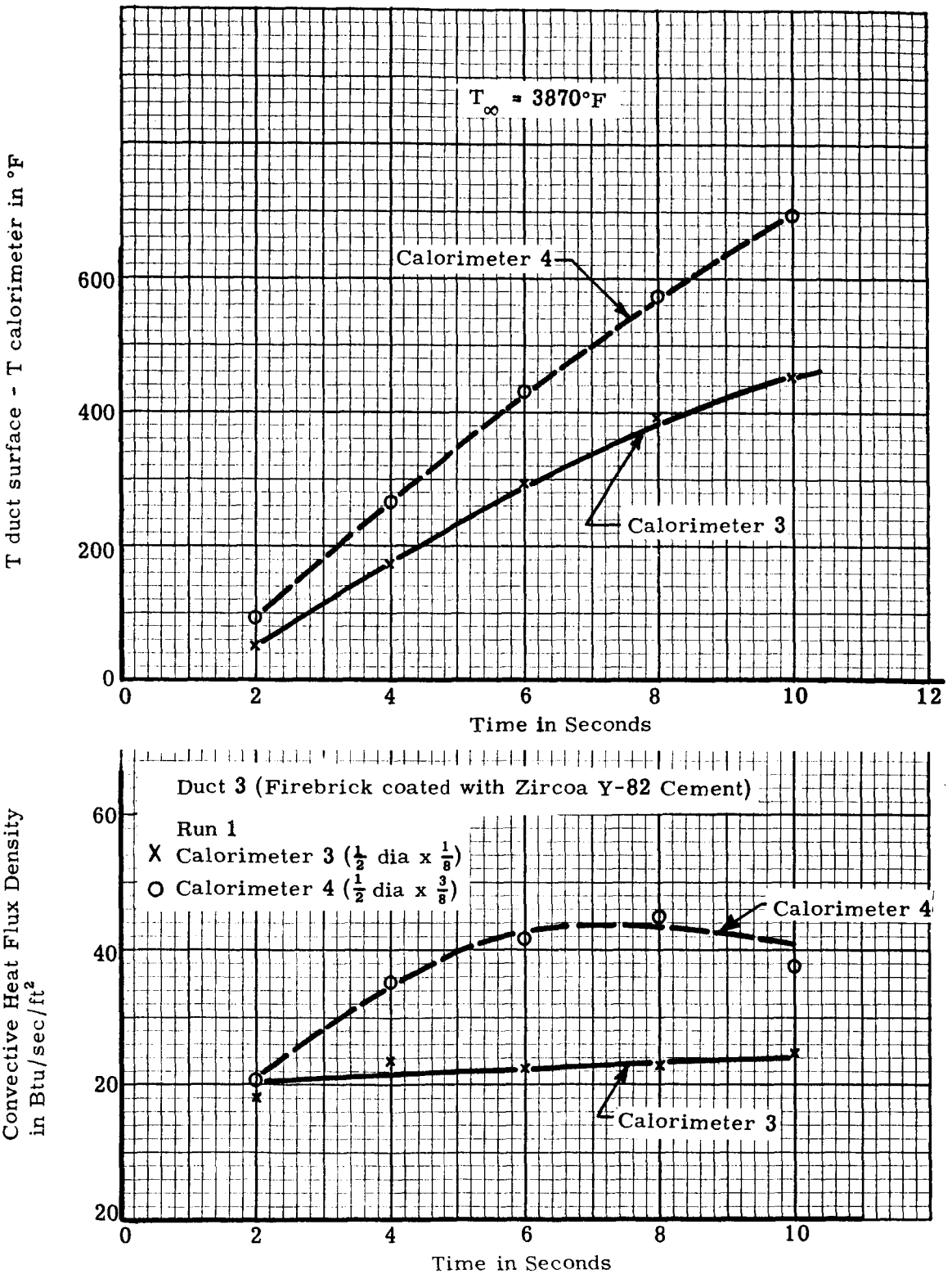

Figure 10. Experimental Convective Heat Flux Densities and Surface Temperature Discontinuities Measured by Slug Calorimeter with Different $(\frac{W}{A})$ Ratios–Duct 3

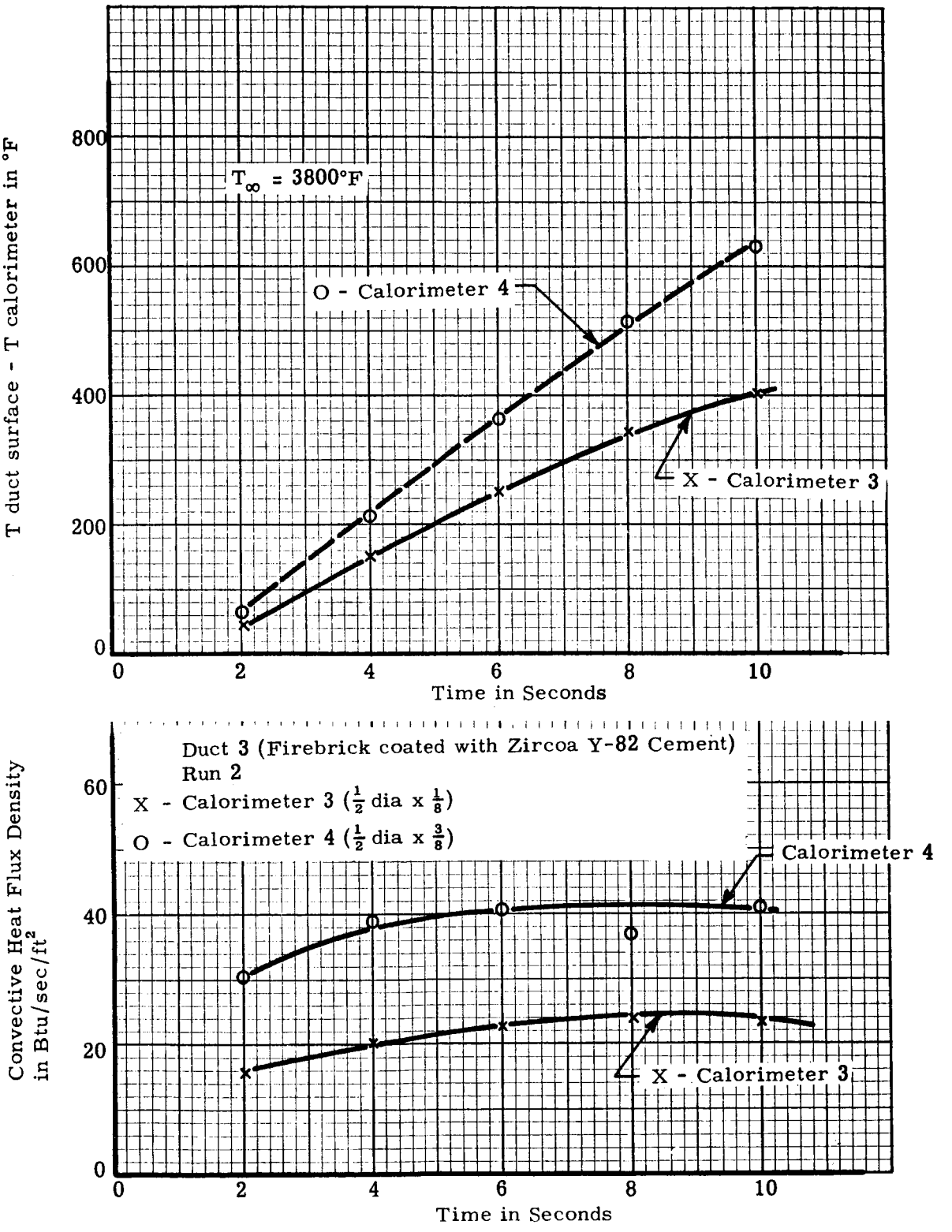

Figure 11. Experimental Convective Heat Flux Densities and Surface Temperature Discontinuities Measured by Slug Calorimeters with Different $(\frac{W}{A})$ Ratios– Duct 3

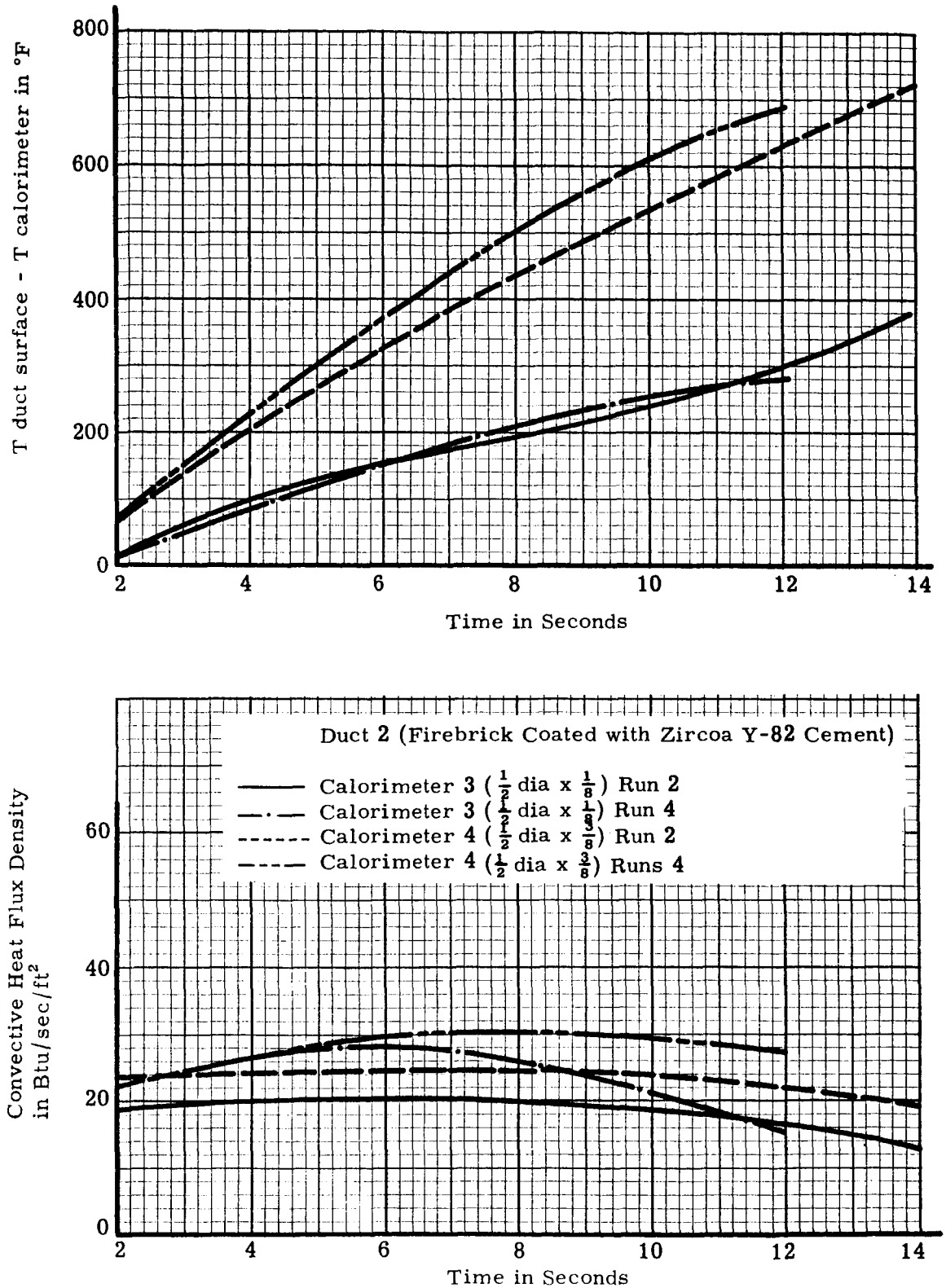

Figure 12. Composite Plot of Experimental Heat Flux Densities and Surface Temperature Discontinuities Measured for Runs in Duct 2

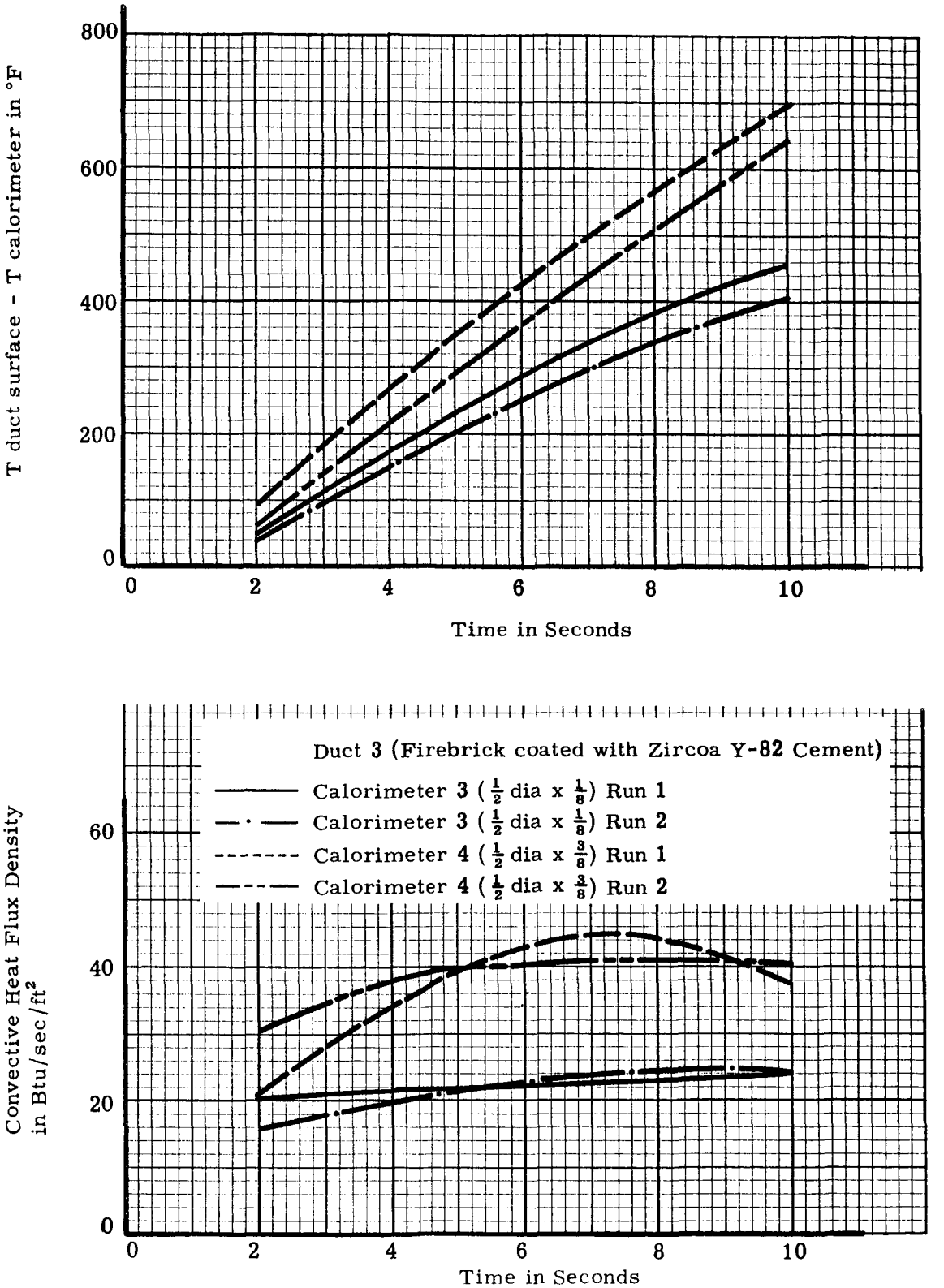

Figure 13. Composite Plot of Experimental Heat Flux Densities and Surface Temperature Discontinuities Measured for Runs in Duct 3

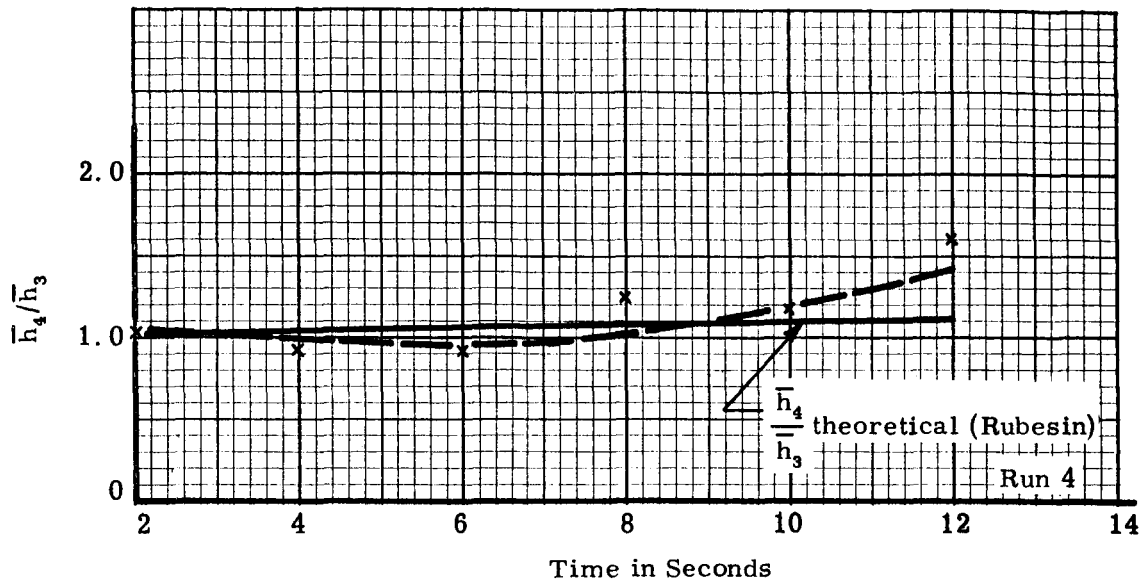

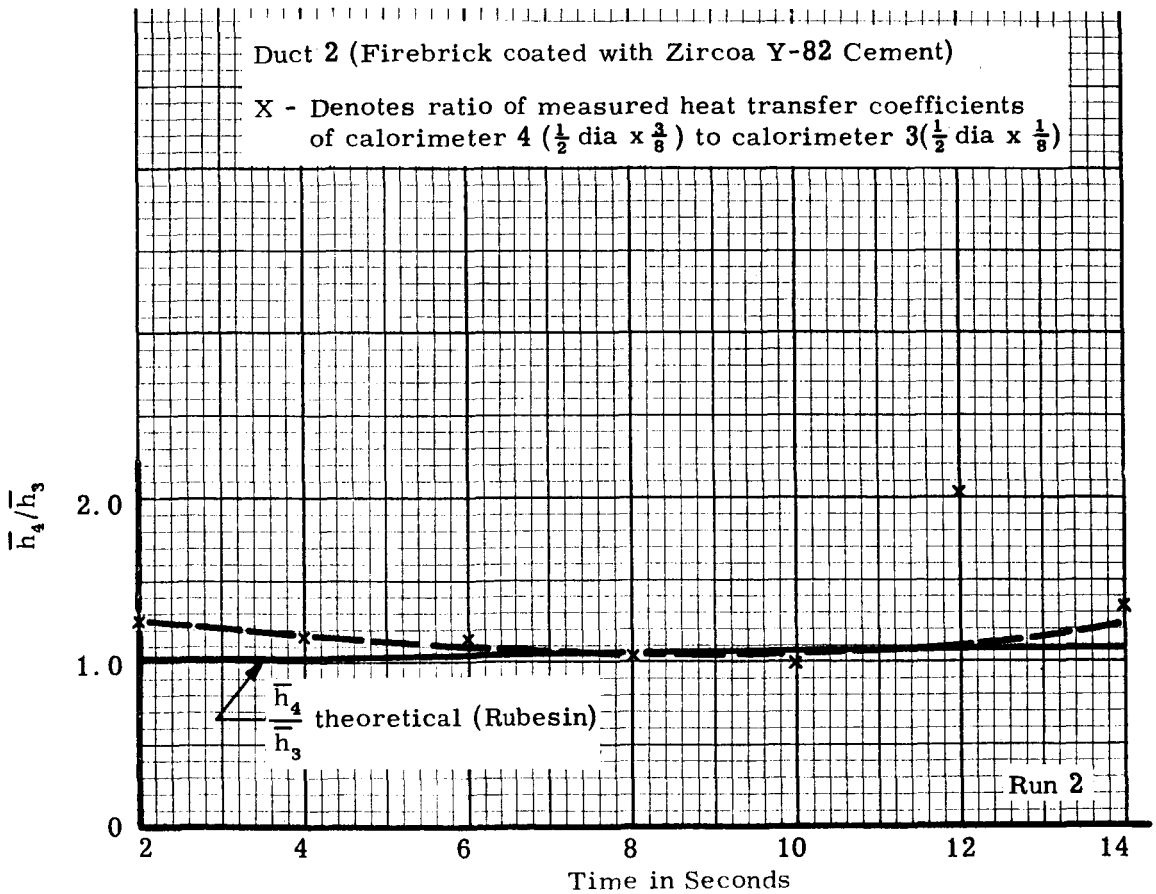

Figure 14. Comparison of Measured and Theoretical Ratios of Heat Transfer Coefficients for Slug Calorimeters with Different $(\frac{W}{A})$ Ratios — Duct 2

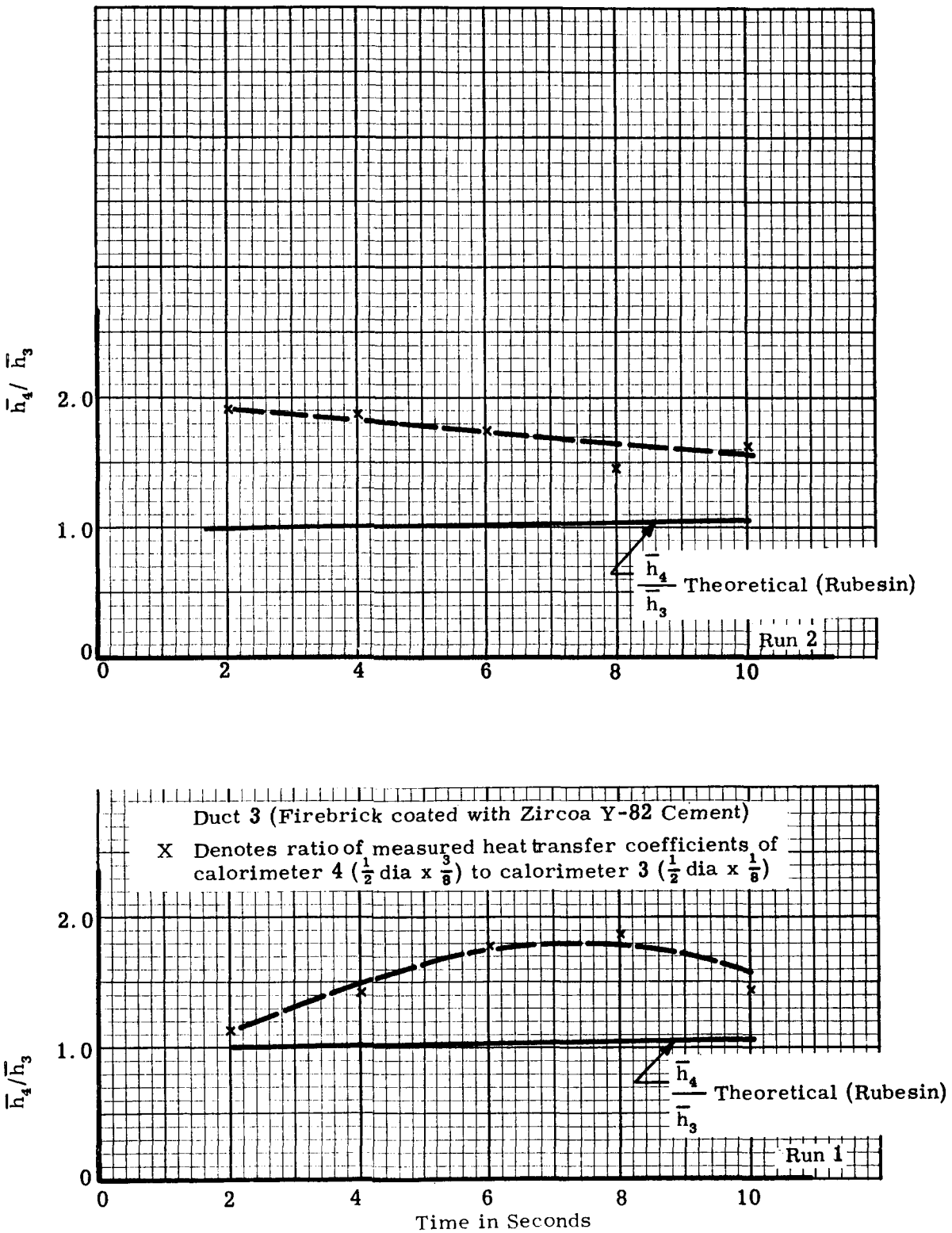

Figure 15. Comparison of Measured and Theoretical Ratios of Heat Transfer Coefficients for Slug Calorimeters with Different $(\frac{W}{A})$ Ratios — Duct 3

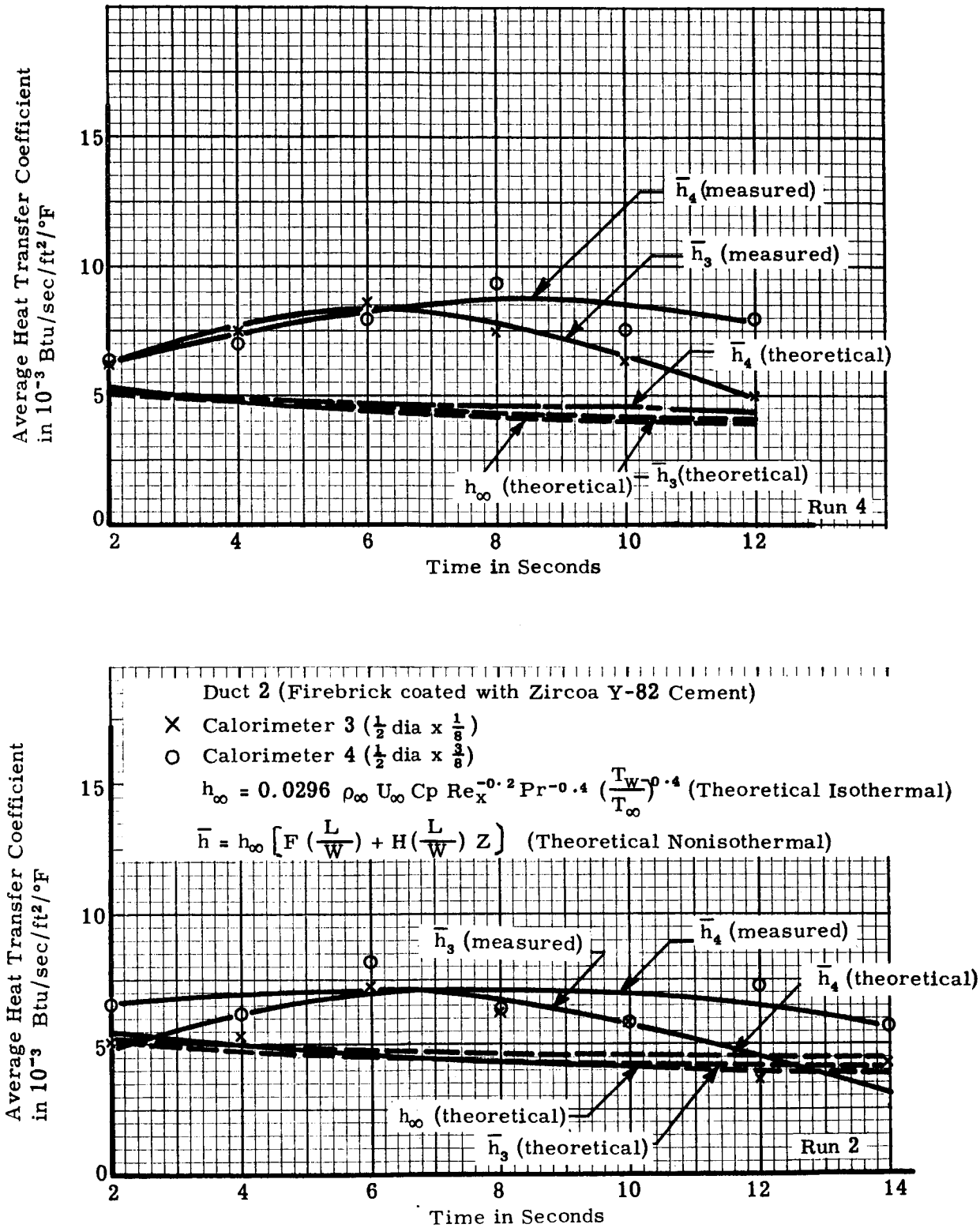

Figure 16. Comparison of Theoretical and Experimental Average Heat Transfer Coefficients for Slug Calorimeters with Different $(\frac{W}{A})$ Ratios — Duct 2

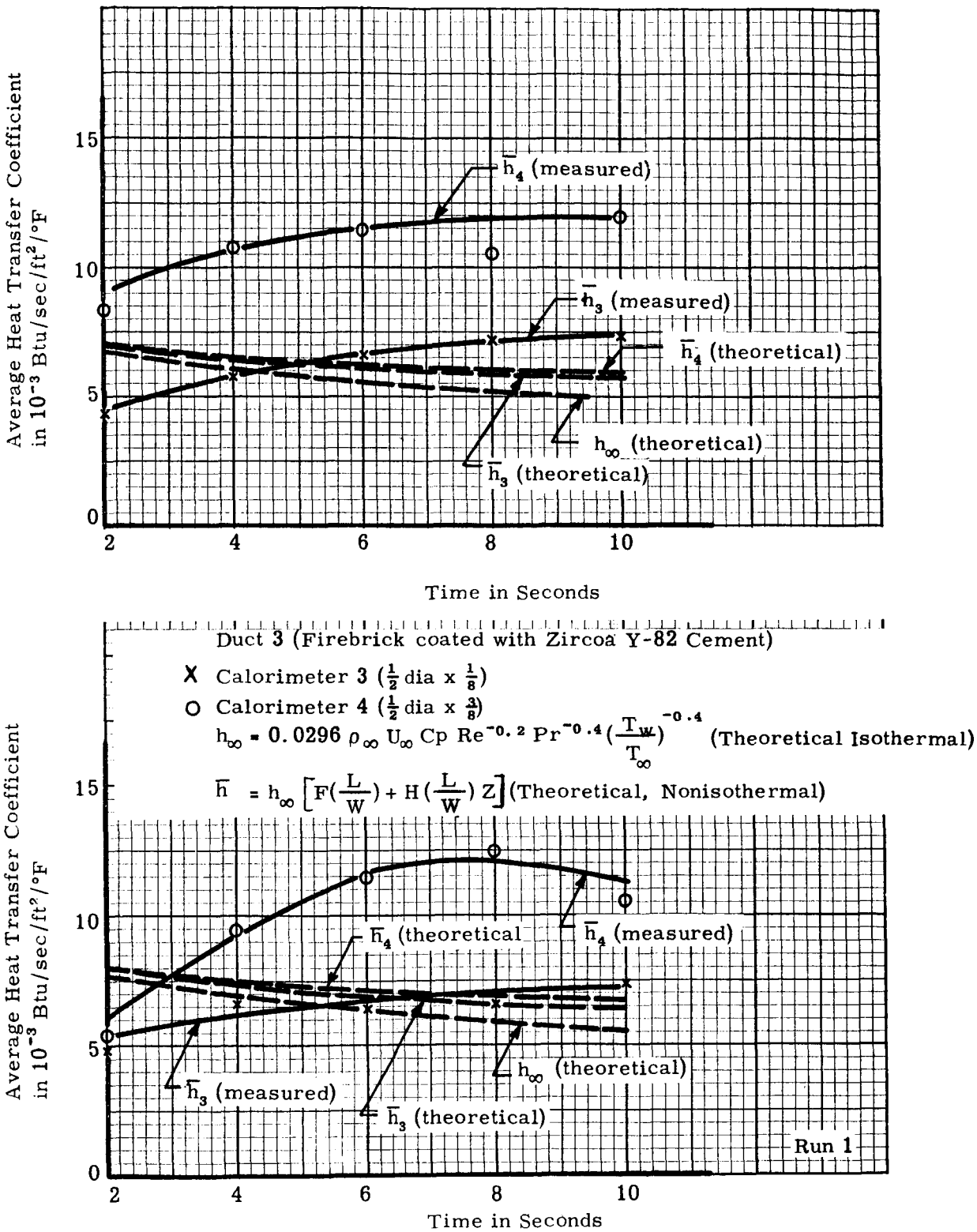

Figure 17. Comparison of Theoretical and Experimental Average Heat Transfer Coefficients for Slug Calorimeters with Different ($\frac{W}{A}$) Ratios— Duct 3

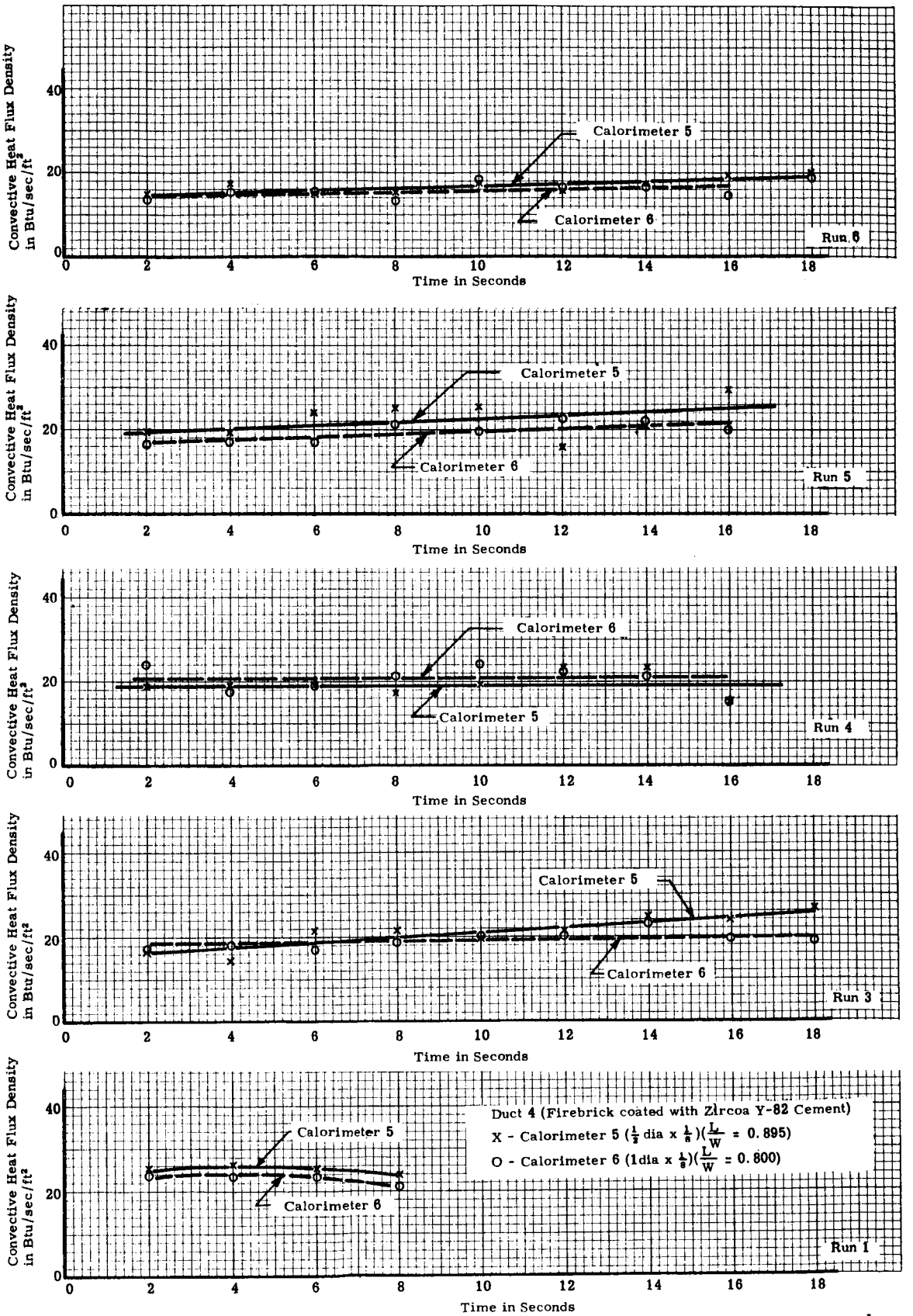

Figure 18. Experimental Convective Heat Flux Densities Measured by Slug Calorimeters with Different $(\frac{L}{W})$ Ratios—Duct 4

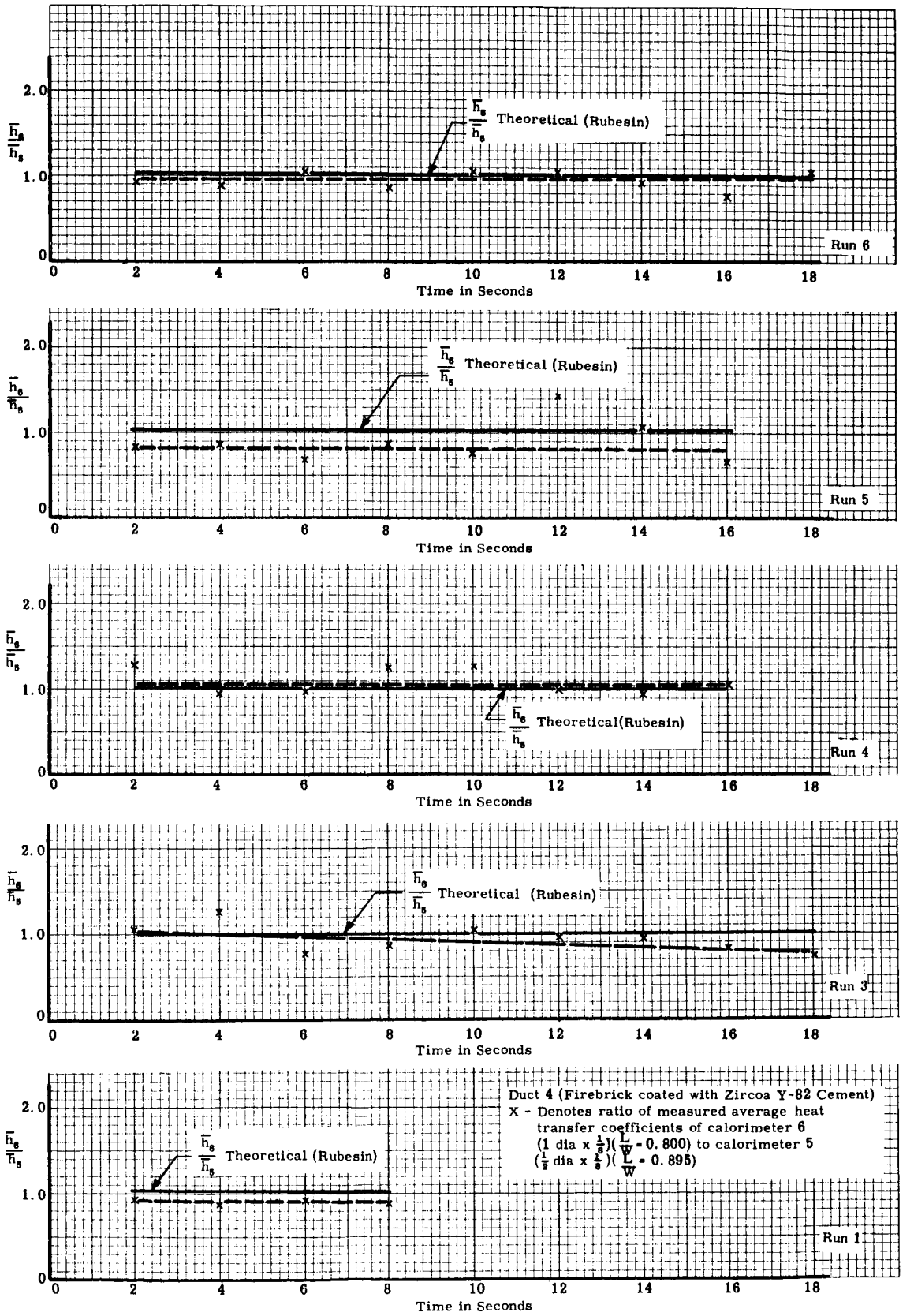

Figure 19. Comparison of Theoretical and Measured Ratios of Heat Transfer Coefficients for Slug Calorimeter with Different $(\frac{L}{W})$ Ratios—Duct 4

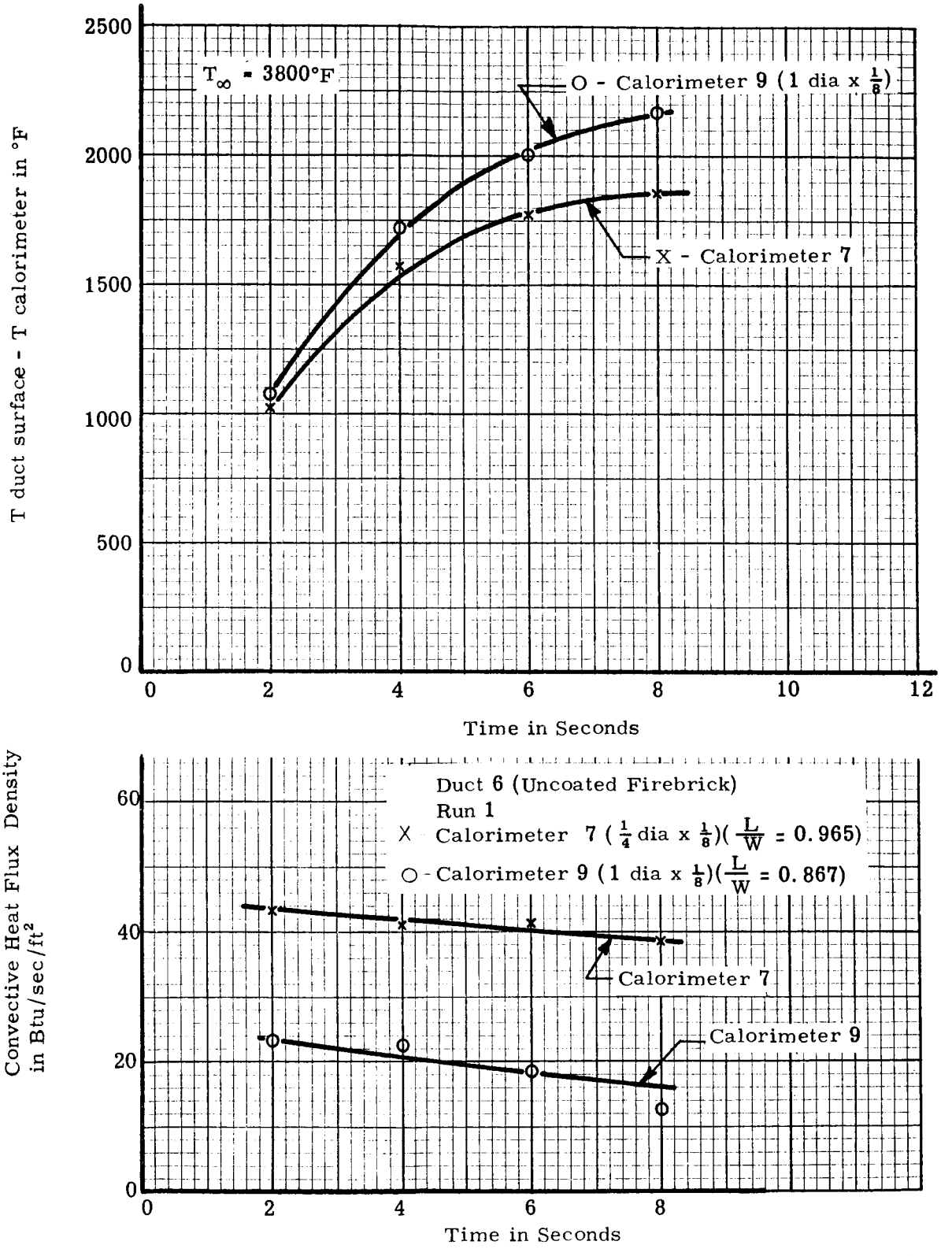

Figure 20. Experimental Convective Heat Flux Densities Measured by Slug Calorimeters with Different $(\frac{L}{W})$ Ratios

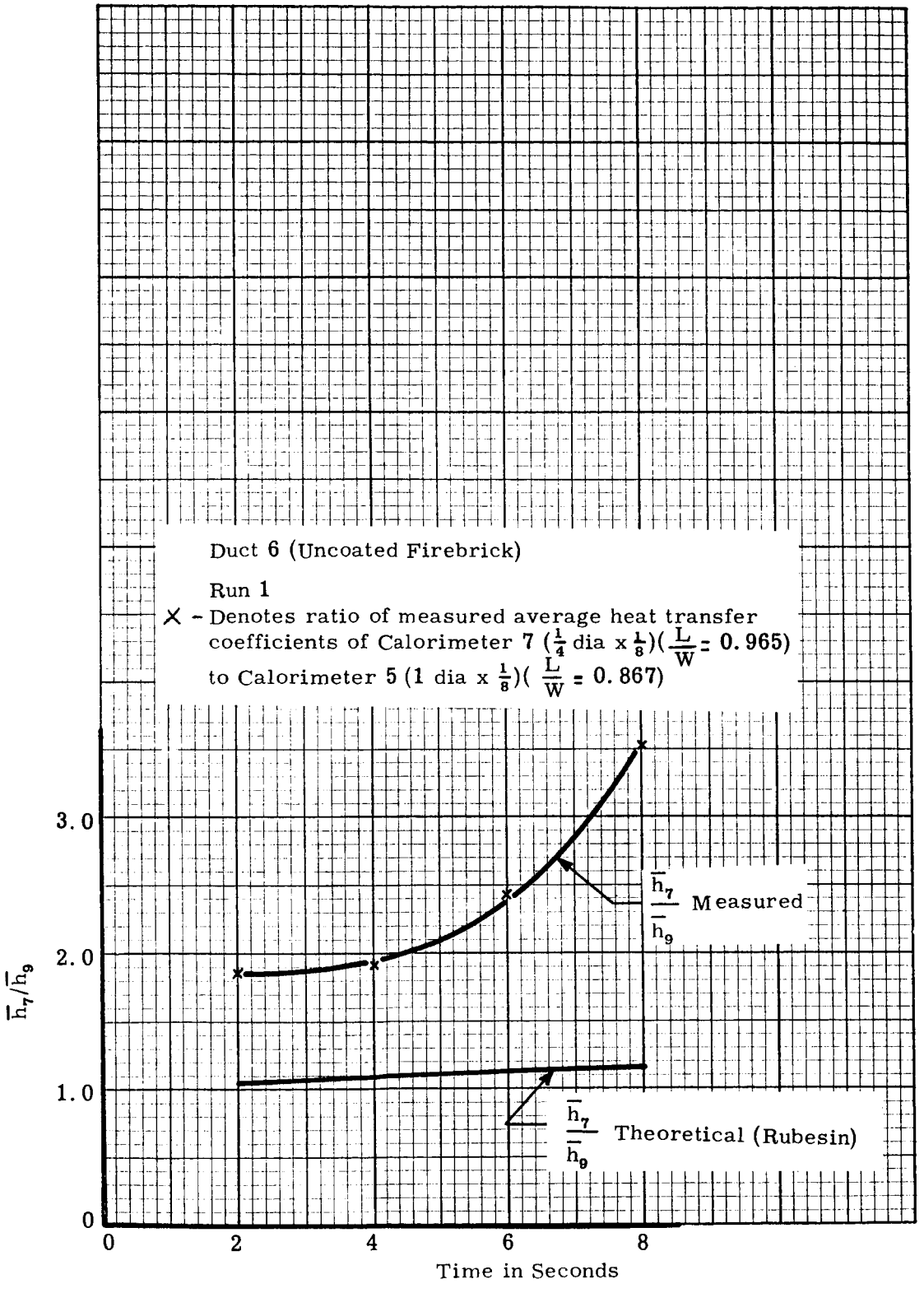

Figure 21. Comparison of Theoretical and Measured Ratios of Heat Transfer Coefficients for Slug Calorimeters with Different $(\frac{L}{W})$ Ratios–Duct 6

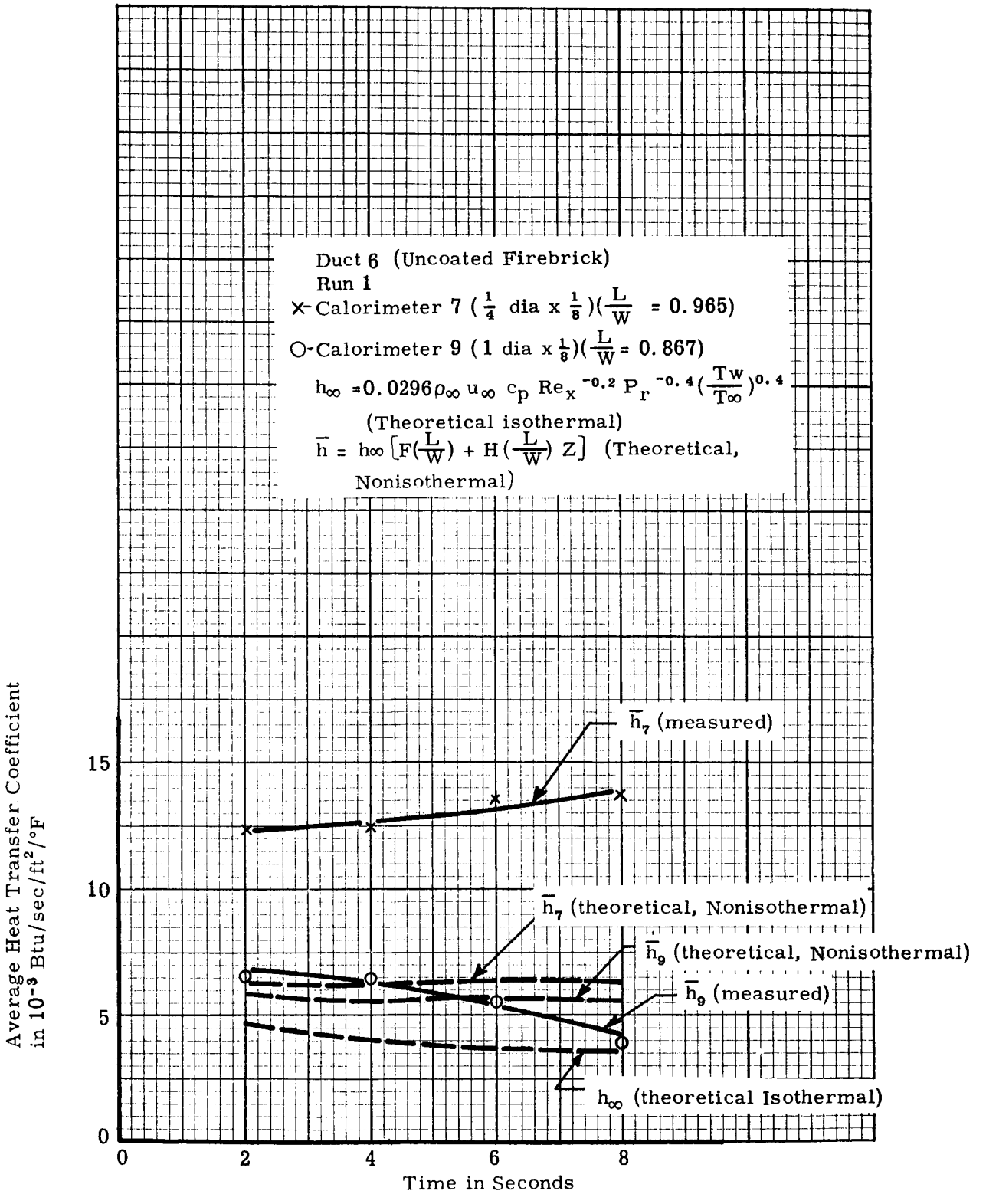

Figure 22. Comparison of Measured and Theoretical Heat Transfer Coefficients for Slug Calorimeters with Different ($\frac{L}{W}$) Ratios—Duct 6

Table 1

Theoretical Heat Flux Parameters for Typical Test Condition

Surface	Temperature °F	Emissivity	Radiative Heat Flux Density Btu/sec/ft^2	Convective Heat Flux Density Btu/sec/ft^2	Total Heat Flux Density Btu/sec/ft^2	Comparison of Calorimeter Indications $\frac{q_m - q_s}{q_s} \times 100$ (1) %	Error (2) %	Convective Heat Transfer Coefficient Btu/hr/ft^2/°F
Membrane Calorimeter	300	0.9	36	104	140	30	40	100
Slug Calorimeter	1500	0.9	35	72	107		8	100
Insulated Surface	1700	0.9	36	64	100			100
Flame	4000	0.2						

Notes:

[1] Subscripts m and s refer to membrane and slug calorimeters, respectively.

[2] Percent error is % deviation from heat flux density to surrounding insulated surface.

Table 2

Theoretical Heat Flux Parameters for Typical Flight Condition

Surface	Temperature °F	Emissivity	Radiative Heat Flux Density Btu/sec/ft^2	Convective Heat Flux Density Btu/sec/ft^2	Total Heat Flux Density Btu/sec/ft^2	Comparison of Calorimeter Indications $\frac{q_m - q_s}{q_s} \times 100$ [1] %	Error [2] %	Convective Heat Transfer Coefficient Btu/hr/ft^2/°F
Membrane Calorimeter	300	0.9	166	195	361	13	41.5	123
Slug Calorimeter	1500	0.9	166	154	320		25.5	123
Insulated Surface	3000	0.9	153	102	255			123
Flame	6000	0.2						

Notes:

[1] Subscripts m and s refer to membrane and slug calorimeters, respectively.

[2] Percent error is percent deviation from heat flux to insulated surface.

Table 3

Summary of Information on Experimental Runs

Duct No.	Run No.	Calorimeter No. and Dimensions	$\frac{L}{W}$	Distance from Tangent Point to Calorimeter	Distance from Burner Nozzle to Calorimeter $\mathcal{C}_L$	Remarks
1	1	#1 - $\frac{1}{4}$ dia. x $\frac{3}{8}$ #2 - $\frac{1}{2}$ dia. x $\frac{1}{8}$	0.800 0.800	4.5 in.	$9\frac{21}{32}$ in.	Data not presented because the calorimeters were uninsulated and gave erroneous data.
	2	#1 - $\frac{1}{4}$ dia. x $\frac{3}{8}$ #2 - $\frac{1}{2}$ dia. x $\frac{1}{8}$	0.800 0.800	4.5 in	$9\frac{21}{32}$ in.	
2	1	#3 - $\frac{1}{2}$ dia. x $\frac{1}{8}$ #4 - $\frac{1}{2}$ dia. x $\frac{3}{8}$	0.935 0.935	7.375 in.	$9\frac{21}{32}$ in.	Gas temperature thermocouple did not read
	2	#3 - $\frac{1}{2}$ dia. x $\frac{1}{8}$ #4 - $\frac{1}{2}$ dia. x $\frac{3}{8}$	0.935 0.935	7.375 in.	$9\frac{21}{32}$ in.	Data appears good
	3	#3 - $\frac{1}{2}$ dia. x $\frac{1}{8}$ #4 - $\frac{1}{2}$ dia. x $\frac{3}{8}$	0.935 0.935	7.375 in.	$9\frac{21}{32}$ in.	Calorimeter 3 did not read
	4	#3 - $\frac{1}{2}$ dia. x $\frac{1}{8}$ #4 - $\frac{1}{2}$ dia. x $\frac{3}{8}$	0.935 0.935	7.375 in.	$9\frac{21}{32}$ in.	Data appears good
3	1	#3 - $\frac{1}{2}$ dia. x $\frac{1}{8}$ #4 - $\frac{1}{2}$ dia. x $\frac{3}{8}$	0.800 0.800	4.5 in.	$6\frac{9}{16}$ in.	Data questionable because of seemingly erratic behavior of Calorimeter 3
	2	#3 - $\frac{1}{2}$ dia. x $\frac{1}{8}$ #4 - $\frac{1}{2}$ dia. x $\frac{3}{8}$	0.800 0.800	4.5 in.	$6\frac{9}{16}$ in.	
4	1	#5 - $\frac{1}{2}$ dia. x $\frac{1}{8}$ #6 - 1 dia. x $\frac{1}{8}$	0.895 0.800	4.5 in.	$9\frac{3}{8}$ in.	All data presented except Run 2 for which gas thermocouple did not read
	2	#5 - $\frac{1}{2}$ dia. x $\frac{1}{8}$ #6 - 1 dia. x $\frac{1}{8}$	0.895 0.800	4.5 in.	$9\frac{3}{8}$ in.	
	3	#5 - $\frac{1}{2}$ dia. x $\frac{1}{8}$ #6 - 1 dia. x $\frac{1}{8}$	0.895 0.800	4.5 in.	$9\frac{3}{8}$ in.	
	4	#5 - $\frac{1}{2}$ dia. x $\frac{1}{8}$ #6 - 1 dia. x $\frac{1}{8}$	0.895 0.800	4.5 in.	$9\frac{3}{8}$ in.	
	5	#5 - $\frac{1}{2}$ dia. x $\frac{1}{8}$ #6 - 1 dia. x $\frac{1}{8}$	0.895 0.800	4.5 in.	$9\frac{3}{8}$ in.	
	6	#5 - $\frac{1}{2}$ dia. x $\frac{1}{8}$ #6 - 1 dia. x $\frac{1}{8}$	0.895 0.800	4.5 in.	$9\frac{3}{8}$ in.	
5	1	#7 - $\frac{1}{4}$ dia. x $\frac{1}{8}$ #9 - 1 dia. x $\frac{1}{8}$	0.950 0.814	4.875	$7\frac{3}{16}$ in.	Temperature of $\frac{1}{4}$ dia calorimeter kept rising at end of testing. Runs 2, 3, and 4 made in order to see if this behavior continued. All runs indicated heat fluxes which appeared far too low and it was concluded that the calorimeter was improperly installed in the duct
	2	#7 - $\frac{1}{4}$ dia. x $\frac{1}{8}$ #9 - 1 dia. x $\frac{1}{8}$	0.950 0.814	4.875	$7\frac{3}{16}$ in.	
	3	#7 - $\frac{1}{4}$ dia. x $\frac{1}{8}$ #9 - 1 dia. x $\frac{1}{8}$	0.950 0.814	4.875	$7\frac{3}{16}$ in.	
	4	#7 - $\frac{1}{4}$ dia. x $\frac{1}{8}$ #9 - 1 dia. x $\frac{1}{8}$	0.950 0.814	4.875	$7\frac{3}{16}$ in.	
6	1	#7 - $\frac{1}{4}$ dia. x $\frac{1}{8}$ #9 - 1 dia. x $\frac{1}{8}$	0.965 0.867	7 in.	9 in.	Data appeared good. Calorimeter data recorded on Moseley X-Y recorder. $\frac{1}{4}$ dia calorimeter went to top of scale before end of testing; could not observe temperature decay. 1 dia calorimeter temperature decayed very slowly indicating good insulation. Firebrick surface melted and prevented further runs in this duct. Melting corresponded well with measured surface temperature.

Table 4

Experimental Data Summary for Duct 2
(Firebrick coated with Zirconium Oxide Cement, Zicoa Y-82)

Calorimeter Data

Cal No.	Size	(L/W)	F(L/W)	H(L/W)
3	$\frac{1}{2}$ dia x $\frac{1}{8}$	.935	1.0118	1.028
4	$\frac{1}{2}$ dia x $\frac{1}{8}$	.935	1.0118	1.028

Distance from tangent point to $\mathcal{C}_L$ calorimeter = 7.375 in.

Run No.	Gas Velocity and Duct Reynold's No.	Time (sec)	Calorimeter Temperature T_{cal} (°F) Cal No. 3	Calorimeter Temperature T_{cal} (°F) Cal No. 4	Surface Temperature T_s (°F)	Temperature Difference Across Boundary Layer $T_{gas} - T_{cal}$ (°F) Cal No. 3	Temperature Difference Across Boundary Layer $T_{gas} - T_{cal}$ (°F) Cal No. 4	Total Measured Heat Flux Density Btu/sec/ft² Cal No. 3	Total Measured Heat Flux Density Btu/sec/ft² Cal No. 4	Radiant Heat Flux Density Btu/sec/ft² Cal No. 3	Radiant Heat Flux Density Btu/sec/ft² Cal No. 4	Convective Heat Flux Density Btu/sec/ft² Cal No. 3	Convective Heat Flux Density Btu/sec/ft² Cal No. 4	Average Heat Flux Coefficient Btu/sec/ft²/°F Cal No. 3	Average Heat Flux Coefficient Btu/sec/ft²/°F Cal No. 4	Ratio of Measured Heat Transfer Coefficients $\bar{h}_4/\bar{h}_3$	Z $\frac{T_s - T_{cal}}{T_{gas} - T_{cal}}$ Cal No. 3	Z Cal No. 4	$\bar{h}/h_\infty$ Predicted by Rubesin's Equation Cal No. 3	$\bar{h}/h_\infty$ Predicted by Rubesin's Equation Cal No. 4	Theoretical Ratio of Heat Transfer Coefficient Predicted by Rubesin's Equation $\bar{h}_4/\bar{h}_3$
2	U_∞ = 148 ft/sec Re_D = 2320	2	155	109	172	3565	3611	25.0	30.3	6.5	6.5	18.5	23.8	0.0052	0.0066	1.27	0.0048	0.0174	0.95	0.96	1.01
		4	250	146	352	3470	3574	24.9	28.9	6.5	6.5	18.4	22.4	0.0053	0.0062	1.17	0.0294	0.0576	0.97	1.00	1.03
		6	345	188	520	3375	3532	30.8	35.6	6.5	6.5	24.3	29.1	0.0072	0.0082	1.14	0.0519	0.0940	0.99	1.04	1.04
		8	455	229	649	3265	3491	26.9	29.2	6.7	6.7	20.2	22.5	0.0062	0.0064	1.03	0.0594	0.1203	1.00	1.06	1.06
		10	548	265	788	3172	3455	26.1	27.8	7.3	7.3	18.8	20.5	0.0059	0.0059	1.00	0.0757	0.1514	1.02	1.10	1.08
		12	625	300	939	3095	3420	19.3	32.9	8.1	8.1	11.2	24.8	0.0036	0.0073	2.03	0.1015	0.1868	1.05	1.13	1.08
		14	690	337	1070	3030	3383	21.9	28.1	8.9	8.9	13.0	19.2	0.0043	0.0057	1.33	0.1254	0.2167	1.07	1.16	1.09
4	U_∞ = 150 ft/sec Re_D = 2260	2	175	108	184	3635	3702	28.9	30.3	6.5	6.5	22.4	23.8	0.0062	0.0064	1.03	0.0024	0.0205	0.94	0.96	1.02
		4	287	145	380	3523	3665	32.8	32.1	6.5	6.5	26.3	25.6	0.0075	0.0070	0.93	0.0263	0.0641	0.97	1.01	1.04
		6	403	183	562	3407	3627	35.7	35.5	6.5	6.5	29.2	29.0	0.0086	0.0080	0.93	0.0466	0.1044	0.99	1.05	1.06
		8	522	230	730	3288	3580	31.7	40.7	7.0	7.0	24.7	33.7	0.0075	0.0094	1.25	0.0532	0.1396	1.01	1.08	1.08
		10	629	274	880	3181	3536	28.2	34.4	7.7	7.7	20.5	26.7	0.0064	0.0076	1.19	0.0789	0.1713	1.02	1.12	1.09
		12	735	320	1000	3075	3490	23.8	36.3	8.5	8.5	15.3	27.8	0.0050	0.0080	1.60	0.0861	0.1948	1.03	1.14	1.11

Table 5

Experimental Data Summary for Duct 3
(Firebrick coated with Zirconium Oxide Cement, Zircoa Y-82)

Calorimeter Data

Cal. No.	Size	(L/W)	F(L/W)	H(L/W)
3	$\frac{1}{2}$ dia x $\frac{1}{6}$	.895	1.0219	0.829
4	$\frac{1}{2}$ dia x $\frac{1}{8}$	.895	1.0219	0.829

Distance from tangent point to $\mathcal{L}$ calorimeters = 4.5 in.

Run No.	Gas Velocity and Duct Reynold's No.	Time (sec)	Calorimeter Temperature T_{cal} (°F) Cal No. 3	Cal No. 4	Surface Temperature T_s (°F)	Temperature Difference Across Boundary Layer $T_{gas} - T_{cal}$ (°F) Cal No. 3	Cal No. 4	Total Measured Heat Flux Density Btu/sec/ft² Cal No. 3	Cal No. 4	Radiant Heat Flux Density Btu/sec/ft² Cal No. 3	Cal No. 4	Convective Heat Flux Density Btu/sec/ft² Cal No. 3	Cal No. 4	Average Heat Flux Coefficient Btu/sec/ft²/°F Cal No. 3	Cal No. 4	Ratio of Measured Heat Transfer Coefficients $\bar{h}_4/\bar{h}_3$	$\frac{T_s - T_{cal}}{T_{gas} - T_{cal}}$ Cal No. 3	Cal No. 4	$\bar{h}/h_\infty$ Predicted by Rubesin's Equation Cal No. 3	Cal No. 4	Theoretical Ratio of Heat Transfer Coefficient Predicted by Rubesin's Equation $\bar{h}_4/\bar{h}_3$
1	U_∞ = 206 ft/sec Re_D = 3060	2	157	116	210	3713	3754	24.5	27.2	6.5	6.5	18.0	20.7	0.0048	0.0055	1.15	0.0142	0.025	1.03	1.04	1.01
		4	250	160	425	3620	3710	30.4	41.8	6.5	6.5	23.9	35.3	0.0066	0.0095	1.44	0.048	0.071	1.06	1.08	1.02
		6	355	217	650	3515	3653	29.2	48.6	6.7	6.7	22.5	41.9	0.0064	0.0115	1.80	0.084	0.119	1.09	1.12	1.03
		8	455	273	850	3415	3597	30.3	52.4	7.6	7.6	22.7	44.8	0.0066	0.0125	1.89	0.116	0.160	1.12	1.16	1.03
		10	570	330	1025	3300	3540	33.1	46.3	8.6	8.6	24.5	37.7	0.0074	0.0106	1.43	0.138	0.196	1.14	1.19	1.04
2	U_∞ = 180 ft/sec Re_D = 2760	2	180	160	223	3620	3640	22.4	35.9	6.5	6.5	15.9	30.4	0.0044	0.0084	1.91	0.012	0.017	1.03	1.04	1.00
		4	271	206	420	3529	3594	26.6	45.4	6.5	6.5	20.1	38.9	0.0057	0.0108	1.89	0.042	0.060	1.06	1.07	1.01
		6	375	260	625	3525	3540	29.3	47.4	6.7	6.7	22.6	20.7	0.0066	0.0115	1.74	0.079	0.103	1.08	1.11	1.02
		8	484	312	825	3316	3488	31.5	44.5	7.5	7.5	24.0	27.0	0.0072	0.0106	1.47	0.103	0.147	1.11	1.14	1.03
		10	599	368	1000	3201	3432	32.1	49.8	8.5	8.5	23.6	41.3	0.0074	0.0120	1.62	0.125	0.184	1.13	1.18	1.04

Table 6

Experimental Data Summary for Duct 4
(Firebrick coated with Zirconium Oxide Cement, Zircoa Y-82)

Calorimeter Data

Cal. No.	Size	(L/W)	F(L/W)	H(L/W)
5	$\frac{1}{2}$" dia x $\frac{1}{8}$"	0.895	1.0219	0.829
6	$\frac{1}{2}$" dia x $\frac{1}{8}$"	0.895	1.0219	0.829

Distance from tangent point to ℄ calorimeter = 4.5 in.

Run No.	Gas Velocity and Duct Reynold's No.	Time (sec)	Calorimeter Temperature T_{cal} (°F) Cal No.		Surface Temperature T_s (°F)	Temperature Difference Across Boundary Layer $T_{gas} - T_{cal}$ (°F) Cal No.		Total Measured Heat Flux Density Btu/sec/ft² Cal No.		Radiant Heat Flux Density Btu/sec/ft² Cal No.		Convective Heat Flux Density Btu/sec/ft² Cal No.		Average Heat Flux Coefficient Btu/sec/ft²/°F Cal No.		Ratio of Measured Heat Transfer Coefficients	Z $\frac{T_s - T_{cal}}{T_{gas} - T_{cal}}$ Cal No.		$\bar{h}/h_{\infty}$ Predicted by Rubesin's Equation Cal No.		Theoretical Ratio of Heat Transfer Coefficient Predicted by Rubesin's Equation
			5	6		5	6	5	6	5	6	5	6	5	6	$\bar{h}_s/\bar{h}_s$	5	6	5	6	$\bar{h}_s/\bar{h}_s$
1	Re_D 2500	2	159	150	210	3641	3650	32.2	30.3	6.5	6.5	25.7	23.8	0.0071	0.0065	0.92	0.014	0.016	1.03	1.05	1.02
		4	275	272	372	3525	3528	32.8	29.9	6.5	6.5	26.3	23.4	0.0075	0.0066	0.88	0.028	0.028	1.05	1.06	1.02
		6	400	387	505	3400	3413	32.3	29.9	6.5	6.5	25.8	23.4	0.0076	0.0069	0.91	0.031	0.035	1.05	1.07	1.02
		8	517	503	630	3283	3297	30.7	27.8	6.7	6.7	24.0	21.1	0.0073	0.0064	0.88	0.034	0.039	1.05	1.07	1.02
3	Re_D 2500	2	167	162	239	3583	3588	22.6	23.3	6.5	6.5	16.1	16.8	0.0045	0.0047	1.04	0.020	0.021	1.04	1.06	1.02
		4	246	262	387	3504	3488	20.7	24.7	6.5	6.5	14.2	18.2	0.0041	0.0052	1.27	0.040	0.036	1.06	1.07	1.01
		6	334	352	516	3416	3398	28.2	23.5	6.5	6.5	21.7	17.0	0.0064	0.0050	0.78	0.053	0.048	1.07	1.07	1.00
		8	426	455	538	3324	3295	28.0	24.9	6.5	6.5	21.5	18.4	0.0065	0.0056	0.86	0.034	0.025	1.05	1.06	1.01
		10	515	558	718	3235	3192	26.7	27.0	7.0	7.0	19.7	20.0	0.0061	0.0063	1.03	0.063	0.050	1.07	1.08	1.01
		12	613	655	809	3137	3095	28.8	27.4	7.4	7.4	21.4	20.0	0.0068	0.0065	0.96	0.062	0.050	1.07	1.08	1.01
		14	718	759	895	3032	2991	32.3	30.6	7.8	7.8	24.5	22.8	0.0081	0.0076	0.93	0.058	0.045	1.07	1.07	1.00
		16	812	860	962	2938	3890	32.1	27.7	8.2	8.2	23.9	19.5	0.0081	0.0067	0.83	0.051	0.035	1.06	1.07	1.01
		18	918	960	1038	2832	2790	35.0	27.5	8.7	8.7	26.3	18.8	0.0093	0.0067	0.72	0.042	0.028	1.06	1.06	1.00
4	Re_D 2500	2	147	170	328	3603	3580	25.2	30.5	6.5	6.5	18.7	24.0	0.0052	0.0067	1.29	0.025	0.019	1.04	1.06	1.01
		4	233	260	407	3517	3490	25.6	24.2	6.5	6.5	19.1	17.7	0.0054	0.0051	0.94	0.049	0.042	1.06	1.07	1.01
		6	319	359	547	3431	3391	25.9	25.6	6.5	6.5	19.4	19.1	0.0057	0.0056	0.98	0.066	0.055	1.08	1.08	1.00
		8	415	459	665	3335	3291	24.1	28.2	6.7	6.7	17.4	21.5	0.0052	0.0065	1.25	0.075	0.063	1.01	1.08	1.00
		10	500	560	782	3250	3190	26.7	31.3	7.2	7.2	19.5	24.1	0.0060	0.0076	1.27	0.087	0.070	1.09	1.09	1.00
		12	600	670	872	3150	3080	31.1	30.2	7.7	7.7	23.4	22.5	0.0074	0.0073	0.99	0.086	0.066	1.09	1.09	1.00
		14	700	774	953	3050	2976	31.6	29.5	8.2	8.2	23.4	21.3	0.0077	0.0072	0.94	0.083	0.066	1.09	1.08	0.99
		16	790	874	1038	2960	2876	23.7	23.8	8.6	8.6	15.1	15.2	0.0051	0.0053	1.04	0.084	0.057	1.09	1.08	0.99
5	Re_D 2500	2	155	146	210	3545	3554	26.3	22.7	6.5	6.5	19.8	16.2	0.0056	0.0046	0.82	0.016	0.018	1.04	1.06	1.02
		4	250	242	372	2450	3458	26.2	23.6	6.5	6.5	19.7	17.1	0.0057	0.0049	0.86	0.035	0.038	1.05	1.07	1.02
		6	355	336	507	3345	3364	30.5	23.4	6.5	6.5	24.0	16.9	0.0072	0.0050	0.69	0.045	0.051	1.06	1.08	1.02
		8	454	438	627	3246	3262	31.6	28.1	6.7	6.7	24.9	21.4	0.0077	0.0066	0.86	0.053	0.058	1.07	1.08	1.01
		10	562	543	728	3138	3157	32.6	26.9	7.0	7.0	25.6	19.9	0.0082	0.0063	0.77	0.052	0.058	1.07	1.08	1.01
		12	663	641	810	3037	3059	23.3	30.0	7.4	7.4	15.9	22.6	0.0052	0.0074	1.42	0.048	0.055	1.06	1.08	1.02
		14	770	746	893	2930	2954	28.4	29.9	7.8	7.8	20.6	22.1	0.0070	0.0075	1.07	0.042	0.050	1.06	1.08	1.02
		16	883	853	962	2817	3847	37.9	28.2	8.2	8.2	29.7	20.0	0.0105	0.0070	0.67	0.028	0.038	1.05	1.07	1.02
6	Re_D 2500	2	155	155	225	3405	3405	21.5	20.2	6.5	6.5	15.0	13.7	0.0044	0.0040	0.91	0.021	0.021	1.04	1.06	1.02
		4	239	242	360	3321	3318	24.0	22.1	6.5	6.5	17.5	15.6	0.0053	0.0047	0.89	0.036	0.036	1.05	1.07	1.01
		6	320	330	440	3240	3230	21.5	21.9	6.5	6.5	15.0	15.4	0.0046	0.0048	1.04	0.037	0.034	1.05	1.07	1.01
		8	440	417	573	3160	3143	22.3	20.0	6.5	6.5	15.8	13.5	0.0050	0.0043	0.86	0.055	0.050	1.07	1.08	1.01
		10	482	503	660	3078	3057	24.3	25.2	6.8	6.8	17.5	18.4	0.0057	0.0060	1.05	0.058	0.051	1.07	1.08	1.01
		12	566	592	737	2994	2968	22.9	23.3	7.0	7.0	15.9	16.3	0.0053	0.0055	1.04	0.057	0.049	1.07	1.08	1.01
		14	650	682	808	2910	2878	25.0	23.6	7.4	7.4	17.6	16.2	0.0060	0.0056	0.93	0.054	0.044	1.07	1.07	1.00
		16	733	770	870	2827	2790	27.0	22.3	7.7	7.7	19.3	14.6	0.0068	0.0052	0.76	0.048	0.036	1.06	1.07	1.01
		18	817	856	940	2743	2704	26.1	27.1	8.1	8.1	18.0	19.0	0.0066	0.0070	1.06	0.045	0.031	1.06	1.06	1.00
		20	902	940	995	2658	2620	25.9	25.1	8.5	8.5	17.4	16.6	0.0065	0.0063	0.97	0.035	0.021	1.05	1.06	1.01

Table 7

Experimental Data Summary for Duct 6
(Uncoated Firebrick)

Cal. No.	Size	(L/W)	F(L/W)	H(L/W)
7	$\frac{1}{4}$ dia x $\frac{1}{8}$	0.965	1.007	1.191
9	1 dia x $\frac{1}{8}$	0.867	1.028	0.750

Distance from tangent point to ℄ calorimeters = 7 in.

Run No.	Gas Velocity and Duct Reynold's No.	Time (sec)	Calorimeter Temperature T_{cal} (°F)		Surface Temperature T_s (°F)	Temperature Difference Across Boundary Layer $T_{gas} - T_{cal}$ (°F)		Total Measured Heat Flux Density Btu/sec/ft²		Radiant Heat Flux Density Btu/sec/ft²		Convective Heat Flux Density Btu/sec/ft²		Average Heat Flux Coefficient Btu/sec/ft²/°F		Ratio of Measured Heat Transfer Coefficients	$Z = \frac{T_s - T_{cal}}{T_{gas} - T_{cal}}$		$\bar{h}/h_\infty$ Predicted by Rubesin's Equation		Theoretical Ratio of Heat Transfer Coefficient Predicted by Rubesin's Equation
			Cal No.			Cal No.		Cal No.		Cal No.		Cal No.		Cal No.			Cal No.		Cal No.		
			7	9		7	9	7	9	7	9	7	9	7	9	$\bar{h}_7/\bar{h}_9$	7	9	7	9	$\bar{h}_7/\bar{h}_9$
1	Re_D 2500	2	296	223	1316	3504	3577	53.8	33.8	10.3	10.3	43.5	23.5	0.0124	0.0066	1.88	0.291	0.306	1.35	1.26	1.07
		4	517	368	2082	3283	3432	57.2	38.3	16.0	16.0	41.2	22.3	0.0125	0.0065	1.92	0.477	0.499	1.58	1.40	1.13
		6	750	519	2524	3050	3281	63.6	40.3	22.0	22.0	41.6	18.3	0.0136	0.0056	2.43	0.582	0.611	1.70	1.50	1.13
		8	989	674	2841	2811	3126	68.1	41.8	29.5	29.5	38.6	12.3	0.0137	0.0036	3.51	0.659	0.693	1.79	1.55	1.15

REFERENCES

1. M. W. Rubesin, "The Effect of an Arbitrary Surface Temperature Variation on the Convective Heat Transfer in an Incompressible Turbulent Boundary Layer," NACA TN 2345, April, 1951.

2. S. Scesa, "Experimental Investigation of Convective Heat Transfer to Air from a Flat Plate with a Stepwise Discontinuous Surface Temperature," MS thesis, University of California, Berkeley, California, February, 1951 (Seban analysis reported here).

3. M. Sibulkin, "Heat Transfer to an Incompressible Turbulent Boundary Layer and Estimation of Heat Transfer Coefficients at Supersonic Nozzle Throats," Journal of the Aeronautical Sciences, vol. 23, 1956, pp 162-172.

4. C. Ferrari, "Determination of the Heat Transfer Properties of a Turbulent Boundary Layer in the Case of Supersonic Flow When the Temperature Distribution Along the Constraining Wall is Arbitrarily Assigned," Report No. CAL/GM-807, Contract NOrd-14523, Cornell Aeronautics Laboratory, Buffalo, New York, March, 1954.

5. W. C. Reynolds, W. M. Kays, and S. J. Kline, "Heat Transfer in the Turbulent Incompressible Boundary Layer II - Step Wall-Temperature Distribution," NASA Memorandum 12-2-58W, December, 1958.

6. R. Eichhorn, E. R. G. Eckert, and A. D. Anderson, "An Experimental Study of the Effects of Non-Uniform Wall Temperature on Heat Transfer in Laminar and Turbulent Axisymmetric Flow Along a Cylinder," WADC TR 58-33, University of Minnesota, Minneapolis, Minnesota, July, 1958.

7. "Heat-Flux-Transducer Designs and Effect of Thermal Disturbances on Transducer Performance," Advanced Technology Laboratories, Report No. ATL-D-1217, February, 1964.

8. "Heat-Flux-Transducer Designs and Effect of Thermal Disturbances on Transducer Performance," Advanced Technology Laboratories, Report No. ATL-D-1226, March, 1964.

REFERENCES (continued)

9. "Heat-Flux-Transducer Designs and Effect of Thermal Disturbances on Transducer Performance," Advanced Technology Laboratories, Report No. ATL-D-1240, May, 1964.

10. W. C. Reynolds, W. M. Kays, and S. J. Kline, "Heat Transfer in the Turbulent Incompressible Boundary Layer, I - Constant Wall Temperature," NASA Memorandum 12-1-58W, December, 1958.

11. F. Kreith, "Principles of Heat Transfer," International Textbook Company, Scranton, Pennsylvania, 1958, pp 236-237.